DESIGN OF BENEFICIAL WAVE DYNAMICS FOR ENGINE LIFE AND OPERABILITY ENHANCEMENT

CONTRACT FA9550-07-C-0045

FINAL REPORT

Gregory Hagen
United Technologies Research Center,
MS129-15,
411 Silver Lane,
East Hartford, CT 06108,
tel. 860 610 7794, HagenGS@utrc.utc.com

0.1 Objectives

Specific objectives of the research at United Technologies Research Center (UTRC) are as follows:
(1) Develop methods and tools for uncertainty management in non-linear non-equilibrium models of wave phenomena in the jet engines.
(2) Develop methods and tools for parameter identification and model validation techniques for non-linear non-equilibrium models of wave phenomena in the jet engines.
(3) Develop methods and tools for Design of Beneficial Wave Dynamics for jet engine life and operability enhancement.

0.2 Summary of Accomplishments

The accomplishments of this research program emphasized the more promising directions of points (2) and (3) listed above, where the uncertainty management called out in point (1) was implicitly accommodated in the analysis. A particular emphasis of this research was the identification of nonlinear models based on high-speed video of flame dynamics. This is a key component of the thermo-acoustic feedback model studied extensively in previous AFOSR-sponsored research programs at UTRC. These results are presented in section 1.1.

These concepts were extended to nonlinear model reduction based on tangent space approximations. Here local gramians are empirically computed based on perturbation trajectories. Key components of this research were the development and application of algorithms for approximating the nonlinear manifold for which a data set belongs, and identification of the nonlinear dynamics on the particular manifold. This lead to the concept of a hybrid (switching) locally affine dynamic texture model, based on the local tangent space approximation of the manifold. These results are presented in section 1.2.

Stability Analysis of Systems with Symmetry-Breaking is presented in section 1.3. Here, sufficient conditions are established for a nonlinear PDE model of thermo-acoustics with wave-speed mistuning. In investigating a new approach to stability analysis of the nonlinear thermo-acoustic model we developed the concept of continued fraction convergence as a condition for stability. Initial results are presented for a string of oscillators and the concepts are extended to the application of subsystems connected in a ring structure.

The results of the current research are summarized in 7 journal papers (1 published, 1 accepted, 5 in preparation), 9 conference papers, and another 2 conference papers currently in preparation.

Contents

Chapter 1

Summary of research results

1.1 Empirical Modeling

In this section we discuss results on empirical modeling. The first set of results relate the standard linear dynamic texture modeling framework to the recently introduced concept of dynamic mode decomposition. These results are built on principal component analysis of the data set. The next two results focus on the identification of nonlinear systems and the analysis of metastability with the analysis of the Markov operator governing the transport of distributions on the phase space.

1.1.1 Dynamic Mode Decomposition

Through the singular value decomposition, we show that the eigenmodes computed from dynamic mode decomposition are the same as those computed from a linear dynamic texture model computed from principal component modes. Comparison results are presented based on

Dynamic Mode Decomposition (DMD) is a method that allows the extraction of dynamically relevant flow features from data [66, 69, 68]. The relation of DMD to eigenmodes of the Koopman operator appear in [63].

Consider an ordered sequence of (vectorized) data snapshots $x_k \in \mathbb{R}^M$ where $k = 1, ..., N$ For integers j, k where $j \leq k$, let $\mathbf{X}_j^k = [x_j, \ldots, x_k]$ so

$$\mathbf{X} := \mathbf{X}_1^N = [x_1, \ldots, x_N] := \left[z_1^T, \ldots, z_M^T\right]^T. \tag{1.1}$$

The row vectors $z_l \in \mathbb{R}^N$ can be considered as records of scalar time-series data at a single spatial location indexed by l. In particular

$$\mathbf{X}_1^{N-1} = \begin{bmatrix} z_1(1:N-1) \\ \vdots \\ z_M(1:N-1) \end{bmatrix}, \quad \mathbf{X}_2^N = \begin{bmatrix} z_1(2:N) \\ \vdots \\ z_M(2:N) \end{bmatrix}$$

Suppose that there is a linear model A such that

$$\mathbf{X}_2^N = A\mathbf{X}_1^{N-1}. \tag{1.2}$$

Suppose also that we can write

$$\mathbf{X}_2^N = \mathbf{X}_1^{N-1} S \tag{1.3}$$

where S is the companion matrix

$$S = \begin{bmatrix} 0 & \\ I_{N-2} & s \end{bmatrix} := C + D \tag{1.4}$$

where s is the least squares approximation of $x_N = \mathbf{X}_1^{N-1} s$, so

$$s = \left[\mathbf{X}_1^{N-1^T} \mathbf{X}_1^{N-1} \right]^{-1} \mathbf{X}_1^{N-1^T} x_N, \tag{1.5}$$

and

$$C := \begin{bmatrix} 0 & 1 \\ I_{N-2} & 0 \end{bmatrix}, \quad D := \begin{bmatrix} 0 & \\ 0 & s - e_1 \end{bmatrix}, \quad e_1^T = [1, 0, \ldots, 0]. \tag{1.6}$$

Write the eigen-decomposition of S as

$$SW = W\Omega, \tag{1.7}$$

where the columns of W are the eigenvectors and Ω is a diagonal matrix consisting of the eigenvalues. Then

$$A\mathbf{X}_1^{N-1} W = \mathbf{X}_1^{N-1} SW = \mathbf{X}_1^{N-1} W\Omega \tag{1.8}$$

which implies that $\mathbf{X}_1^{N-1} W$ approximate some of the eigenvectors and Ω approximates some of the eigenvalues of A. We refer to these eigenvectors as DMD modes, denoted by Φ, with

$$\Phi = \mathbf{X}_1^{N-1} W. \tag{1.9}$$

Note that the DMD modes are composed of the normalized columns of W scaled by the data $\mathbf{X}_1^{N-1}$. Therefore, each column of Φ will be scaled according to the data. This is analogous to taking the Fourier transform of a time-series record, where associated with each frequency is a magnitude response. This is discussed further in the next section. Therefore, associated with each DMD eigenvalue will be a magnitude given by the norm of associated column of Φ.

Principal Component Analysis

Principal component analysis (PCA) is also known as proper orthogonal decomposition (POD) [35], Karhunen-Loeve Decomposition [72], and singular value decomposition (SVD) [36]. The SVD of a matrix $\mathbf{X}_1^{N-1}$ is

$$\mathbf{X}_1^{N-1} = U\Sigma V^T, \tag{1.10}$$

where U and V are unitary, $U^T U = I$ and $V^T V = I$. A popular method of computing POD is the method of snapshots. First form the correlation matrix

$$K = \mathbf{X}_1^{N-1^T} \mathbf{X}_1^{N-1} = V\Sigma U^T U\Sigma V^T = V\Lambda V^T, \tag{1.11}$$

where $\Lambda := \Sigma^2$. Through the svd relation, the POD modes U are computed from V as follows:

$$U = \mathbf{X}_1^{N-1} V \Lambda^{-\frac{1}{2}}, \tag{1.12}$$

which is identical to (1.10), however K is of smaller dimension than $\mathbf{X}_1^{N-1}$ and therefore computing V, Λ through (1.11) is sometimes easier than computing (1.10) directly.

Combining (1.5) with (1.10) results in

$$\begin{aligned} s &= \left[\mathbf{X}_1^{N-1^T} \mathbf{X}_1^{N-1}\right]^{-1} \mathbf{X}_1^{N-1^T} x_N \\ &= V \Lambda^{-1} V^T V \Sigma U^T x_N \\ &= V \Sigma^{-1} U^T x_N. \end{aligned} \tag{1.13}$$

From (1.12),

$$\hat{x}_N = \mathbf{X}_1^{N-1} s = \mathbf{X}_1^{N-1} V \Sigma^{-1} U^T x_N = U \Sigma V^T V \Sigma^{-1} U^T x_N = U U^T x_N, \tag{1.14}$$

which implies that the least squares approximation of x_N is precisely the projection of x_N on to the modes U.

Conditioning

The algorithm for computing the eigenvalues of S given by (1.4) is ill-conditioned. Here we discuss the use of SVD as described in [67] to result in a more robust algorithm. We essentially apply equations (1.7, 1.8, 1.10) and apply a similarity transform on S so that

$$\tilde{S} := \Sigma V^T S V \Sigma^{-1}. \tag{1.15}$$

We first combine (1.8, 1.10) to get

$$A U \Sigma V^T W = U \Sigma V^T S W = U \Sigma V^T W \Omega. \tag{1.16}$$

Pre-multiplying (1.16) by U^T and applying (1.15) results in

$$U^T A U \Sigma V^T W = \Sigma V^T S W = \Sigma V^T W \Omega \tag{1.17}$$

$$\begin{aligned} &= \Sigma V^T S V \Sigma^{-1} \Sigma V^T W = \Sigma V^T W \Omega \\ &= \tilde{S} Y = Y \Omega, \end{aligned} \tag{1.18}$$

where $Y := \Sigma V^T W$ is the matrix whose columns are the eigenvectors of $\tilde{S}$. Referring back to the discussion in [67], note that according to (1.17, 1.18), $U^T A U = \tilde{S}$, and the DMD modes are

$$\Phi = UY = U \Sigma V^T W. \tag{1.19}$$

It remains to be shown how to compute $\tilde{S}$ directly from the data. Define $\Theta_1^{N-1} = U^T \mathbf{X}_1^{N-1} = \Sigma V^T = [\theta_1, \ldots, \theta_{N-1}]$ and similarly define $\Theta_j^k = [\theta_j, \ldots, \theta_k]$. First, swap the left and right sides of (1.3) and pre-multiply by U^T and post-multiply by $V\Sigma^{-1}$ to result in, after applying (1.10),

$$\begin{aligned} \tilde{S} = \Sigma V^T S V \Sigma^{-1} &= U^T \mathbf{X}_2^N V \Sigma^{-1} \qquad (1.20) \\ &= U^T \left[U \Sigma V_2^{N-1^T}, x_N \right] V \Sigma^{-1} \\ &= \left[\Theta_2^{N-1}, \theta_N \right] V \Sigma^{-1} \\ &= \Theta_2^N \Theta_1^{N-1^T} \Lambda^{-1}. \qquad (1.21) \end{aligned}$$

The above equations involve computing the SVD of the data $\mathbf{X}$ and projecting the data onto the PCA modes U.

Truncation

The scaling by Λ^{-1} in (1.21) motivates truncating the model because Λ often features singular values with very low magnitude and the high-indexed entries of Θ_1^{N-1}. In other words, the projection of the data on to the higher order PCA modes results in time-series data with very small absolute value, which is the case when the number of snapshots N is smaller than the spatial dimension of the data M, i.e. $N < M$. Suppose that instead of computing the DMD on the snapshot data, we first project on to the low-dimensional space spanned by a truncated set of PCA modes U_r. Equations (1.2,1.3) become

$$\Theta_2^N = U_r^T \mathbf{X}_2^N = U_r^T A \mathbf{X}_1^{N-1} = U_r^T A U_r \Theta_1^{N-1} := A_r \Theta_1^{N-1}. \qquad (1.22)$$

$$\Theta_2^N = U_r^T \mathbf{X}_2^N = U_r^T \mathbf{X}_1^{N-1} S = \Theta_1^{N-1} S, \qquad (1.23)$$

which results in

$$A_r \Theta_1^{N-1} = \Theta_1^{N-1} S. \qquad (1.24)$$

Rearranging (1.24) yields

$$A_r = \Theta_1^{N-1} S V \Sigma^{-1} = \Sigma V^T S V \Sigma^{-1} = \tilde{S}. \qquad (1.25)$$

In particular, by (1.13)

$$\begin{aligned} \tilde{S} &= \left[\Theta_2^{N-1}, \Theta_1^{N-1} s \right] V \Sigma^{-1} \\ &= \left[\Theta_2^{N-1}, \Sigma V^T V \Sigma^{-1} U^T x_N \right] V \Sigma^{-1} \\ &= \left[\Theta_2^{N-1}, \theta_N \right] V \Sigma^{-1} \\ &= \Theta_2^N \Theta_1^{N-1^T} \Lambda^{-1}, \qquad (1.26) \end{aligned}$$

which resembles (1.21). Furthermore, by (1.14),

$$\hat{\theta}_N = U_r^T \hat{x}_N = U_r^T U \Sigma V^T s = \Theta_1^{N-1} s = \Theta_1^{N-1} V \Sigma^{-1} U^T x_N = \Theta_1^{N-1} V \Sigma^{-1} \theta_N. \qquad (1.27)$$

Dynamic Texture Model with PCA

Dynamic texture models are essentially linear dynamic models describing the dynamics of PCA coefficients under the assumption that the driving noise is second order Gaussian (see the work of Soatto et al. [23]). Suppose the data snapshots $\{x_k\}_{k=1,\ldots,N}$ are the output of a linear dynamical system

$$\theta_{k+1} = A\theta_k + Bv_k, \tag{1.28}$$

$$x_k = \Psi\theta_k + w_k, \tag{1.29}$$

where $\Psi = [\Psi_1, \ldots, \Psi_K] \in \mathbb{R}^{n\times K}$ chosen to minimize the objective

$$\min_{\Psi,\Theta} \|\mathbf{X}_1^{N-1} - \Psi\Theta_1^{N-1}\|_F^2. \tag{1.30}$$

Note that in [23] the minimization is based on all N data snapshots and here we leave out the last snapshot. Under the assumption of stationarity, the optimal solutions will be similar in both cases. The minimizing solution of (1.30) is obtained through the SVD of $\mathbf{X}_1^{N-1} = U\Sigma V^T$ by taking

$$\Psi = U, \quad \Theta_1^{N-1} = \Sigma V^T. \tag{1.31}$$

The linear dynamic texture model is found by minimizing the objective

$$\min_A \|\Theta_2^N - A\Theta_1^{N-1}\|_F^2. \tag{1.32}$$

Note that

$$\Theta_2^N = \left[\Theta_2^{N-1}, \theta_N\right] = \left[\Theta_1^{N-1}D_2, U^T x_N\right] = \Theta_1^{N-1}\left[D_2, V\Sigma^{-1}U^T x_N\right], \tag{1.33}$$

where

$$D_2 = \begin{bmatrix} 0 \\ I_{N-2} \end{bmatrix}. \tag{1.34}$$

From (1.13) we have $V\Sigma^{-1}U^T x_N = s$, and combining this with (1.33,1.51) gives

$$\Theta_2^N = \Theta_1^{N-1}S \tag{1.35}$$

The optimal solution of (1.32) is given in closed form by

$$A = \Theta_2^N \Theta_1^{N-1^T}\left[\Theta_1^{N-1}\Theta_1^{N-1^T}\right]^{-1} \tag{1.36}$$

$$= \Theta_1^{N-1}S\Theta_1^{N-1^T}\left[\Theta_1^{N-1}\Theta_1^{N-1^T}\right]^{-1}$$

$$= \Theta_1^{N-1}SV\Sigma\left[\Sigma V^T V\Sigma\right]^{-1}$$

$$= \Theta_1^{N-1}SV\Sigma^{-1}, \tag{1.37}$$

which is the same as (1.25) showing that the dynamic texture model is the same as the linear model used in DMD. By application of the SVD (1.10), another way of writing (1.36) is simply

$$A = \Theta_2^N \Theta_1^{N-1^T}\left[\Sigma V^T V\Sigma\right]^{-1} \tag{1.38}$$

$$= \Theta_2^N \Theta_1^{N-1^T}\Lambda^{-1} = \tilde{S}. \tag{1.39}$$

Following [23], the sample input noise covariance Q is estimated by

$$\hat{Q} = \frac{1}{N}\sum_{i=1}^{N} \hat{v}_i \hat{v}_i^T. \tag{1.40}$$

where $\hat{v}_i = \theta_{i+1} - A\theta_i$. The driving noise input matrix B is estimated such that

$$BB^T = \hat{Q}. \tag{1.41}$$

1.1.2 Nonlinear Model Identification from Spectral Analysis of Markov Operator

We provide a numerical approach to estimating nonlinear stochastic dynamic models from time-series data. After possible dimensional reduction, time-series data can be used to construct an empirical Markov model. Spectral analysis of the Markov model is then carried out to detect the presence of complex limit cycling, almost invariant, and bi-stable behavior in the model. Model parameters are expressed as a linear combination of basis functions over the phase space. A least squares minimization is used to fit the basis function coefficients in order to match the spectral properties of the respective Markov operators. The approach is demonstrated on the estimation of a nonlinear stochastic model describing combustion oscillation data.

We provide an approach for estimating nonlinear dynamic models, possibly driven by noise. The estimation approach is based on comparing the spectral properties of the empirically constructed Markov operator with the model-based Markov operator. A nonlinear model is fit such that its associated Markov operator has similar spectral properties as the empirical Terms in the stochastic differential equation model are estimated by a linear combination of basis functions. The coefficients appear in the numerical approximation of the Markov model, and are fit using least squares minimization. Model validation is motivated spectral methods developed in [53] [51] for the comparison of dynamical systems.

Spectral method for analysis and comparison

In this section, we describe spectral methods for the analysis and comparison of the dynamical systems. The material for this section is taken from [20][53][51]. Also, see [45] for an introduction to these concepts.

Consider the stochastic dynamical system

$$\frac{\partial x}{\partial t} = b(x) + \sigma(x)\xi, \quad x \in X \in \mathbb{R}^d, \tag{1.42}$$

or its discrete time equivalent,

$$x_{k+1} = T(x_k, \xi_k) \tag{1.43}$$

where each $x_k \in X \subset \mathbb{R}^d$ is the state vector and $\xi_k \in U$ is sequence of i.i.d. random noise. Associated with T is a stochastic transition function $p(x, A)$, which gives the transition probability to jump from point $x \in X$ to set $A \in \mathcal{B}(X)$, where $\mathcal{B}(X)$ is the Borel sigma algebra of X. For deterministic dynamics i.e., when $\xi_n = 0$, we have $p(x, A) = \delta_{T(x)}(A)$, where δ is the Dirac delta measure. Stochastic transition

function can be used to define two linear transfer operators called as Perron-Frobenius and Koopman operators. Here we consider the finite dimensional approximation of the P-F operator. To do this we consider the finite partition of the state space X i.e.,

$$\mathcal{X} = \{D_1, ..., D_m\} \tag{1.44}$$

such that $D_i \cap D_j = \emptyset$ for $i \neq j$ and $\cup_{i=1}^{m} D_i = X$. P-F operator on the finite dimensional vector space $\mathbb{R}^m$ can be represented by a matrix $P : \mathbb{R}^m \to \mathbb{R}^m$ as follows:

$$P_{ij} = \frac{\mu_L(T^{-1}(D_j) \cap D_i)}{\mu_L(D_i)}, \quad i, j = 1, ..., m \tag{1.45}$$

The resulting matrix is non-negative and because $T : D_i \to X$, $\sum_{j=1}^{m} P_{ij} = 1$ i.e., P is a Markov or a row-stochastic matrix.

Important complex dynamical features of the dynamical system T can be captured using its Markov matrix P. For example long term or asymptotic behavior of the dynamical system T is captured by the invariant measure or more appropriately physically relevant measure. Finite dimensional approximation of the invariant measure or the outer approximation to the support of the invariant measure can be obtain from the left eigenvector of Markov matrix P with eigenvalue one. i.e.,

$$\mu P = 1 \cdot \mu$$

Similarly the presence of periodic or limit cycling behavior in T can be captured by the complex unitary spectrum and the corresponding eigenvectors of P. Moreover if the Markov matrix P has real eigenvalue close to one then it is the indicator for the presence of almost invariant or bistable behavior in the dynamical system T. For more detail on this topic refer to [19][20].

We outline an approach to numerically approximate the stochastic dynamical system (1.42) based on the empirically obtained Markov matrix P.

Set

$$a_{ij}(x) = \sum_{k=1}^{d} \sigma_{ik}(x)\sigma_{jk}(x) \tag{1.46}$$

Under certain regularity conditions [45], the evolution of the density, ρ under (1.42) satisfies the Fokker-Planck equation,

$$\begin{aligned} \frac{\partial \rho}{\partial t} &= \frac{1}{2} \sum_{i,j=1}^{d} \frac{\partial^2}{\partial x_i \partial x_j}(a_{ij}\rho) - \sum_{i=1}^{d} \frac{\partial}{\partial x_i}(b_i \rho) \\ &:= \mathcal{F}\rho, \quad t > 0, x \in \mathbb{R}^d. \end{aligned} \tag{1.47}$$

Consider the finite-dimensional (discrete-space) approximation of $\mathcal{F}$ by discretizing the underlying phase space X with the partition $\mathcal{X}$ following (1.44). Therefore, the distribution ρ is approximated by a finiite-dimensional vector $u(x) \in \mathbb{R}^m$ and let

$$U = \text{diag}\{u\} \in \mathbb{R}^{m \times m}, \tag{1.48}$$

where $\mathrm{diag}\{u\}$ is a diagonal matrix whose entries are the elements of the vector u. Similarly, the operators are approximated by their finite-dimensional matrices:

$$F \approx \mathcal{F}, \;\; F \in \mathbb{R}^{m \times m}.$$

Continuing this way, write the discretized approximations of $a_i j(x)$ and $b_i(x)$, respectively,

$$a_{ij}(x) \approx A_{ij}(x) \in \mathbb{R}^m, \;\; b_i(x) \approx B_i(x) \in \mathbb{R}^m. \tag{1.49}$$

Similarly we write the discretized differential operators

$$\frac{1}{2}\frac{\partial^2}{\partial x_i \partial x_j} \approx D_{ij}^2 \in \mathbb{R}^{m \times m}, \;\; \frac{\partial}{\partial x_i} \approx D_i \in \mathbb{R}^{m \times m}. \tag{1.50}$$

Next, define the matrices:

$$D^2(U) := \left[D_{11}^2 U, \ldots, D_{ij}^2 U, \ldots, D_{dd}^2 U\right] \in \mathbb{R}^{m \times md^2} \tag{1.51}$$

$$D^1(U) := \left[D_1 U, \ldots, D_i U, \ldots, D_d U\right] \in \mathbb{R}^{m \times md} \tag{1.52}$$

$$D(U) := \left[D^2(U), D^1(U)\right] \in \mathbb{R}^{m \times (md^2 + md)} \tag{1.53}$$

and

$$A := \begin{bmatrix} A_{11} \\ \vdots \\ A_{ij} \\ \vdots \\ A_{dd} \end{bmatrix} \in \mathbb{R}^{md^2}, \quad B := \begin{bmatrix} B_1 \\ \vdots \\ B_j \\ \vdots \\ B_d \end{bmatrix} \in \mathbb{R}^{md},$$

$$C := \begin{bmatrix} A \\ B \end{bmatrix} \in \mathbb{R}^{(md^2 + md)}. \tag{1.54}$$

The infinite-dimensional Fokker-Planck operator is approximated in finite dimensions by

$$\mathcal{F}\rho \approx Fu = D(U)C. \tag{1.55}$$

We next write (1.47) in discrete time, with

$$\frac{\partial u}{\partial t} \approx \frac{u_{t+1} - u_t}{\delta t},$$

where δt is the time step which the time-series data was obtained. Substituting this into the left side of (1.47) results in the Markov matrix appearing equation (1.45),

$$\begin{aligned} u_{t+1} &= u_t + \delta t F u_t \\ &= [u_t + \delta t D(U)C] \\ &:= P u_t. \end{aligned} \tag{1.56}$$

We empirically obtain P directly from data by discretizing the underlying phase space ($\mathbb{R}^d$) to obtain this discrete-space approximation. The spectrum of P is given by $P\mathcal{V} = \mathcal{V}\Lambda$, where

$$\mathcal{V} = [v_0, v_1, v_2, \ldots, v_m], \quad \Lambda = diag(\lambda_0, \lambda_1, \ldots, \lambda_m). \tag{1.57}$$

Under suitable conditions there exists a steady distribution v_0 where $\lambda_0 = 1$.

Consider a single eigenvector $v \in \mathbb{R}^m$ with eigenvalue λ. We have

$$Pv = [v + \delta t D(V)C] = \lambda v, \tag{1.58}$$

and after rearranging,

$$D(V)C = \frac{\lambda - 1}{\delta t} v := w. \tag{1.59}$$

This can be solved for C which will give the functional forms of $b(x)$ and $\sigma(x)$ appearing in (1.42). Of course, for a single eigenvector, there are multiple solutions. We solve (1.59) for multiple eigenpairs; the first k for example. We have

$$\begin{bmatrix} D(V_0) \\ \vdots \\ D(V_{k-1}) \end{bmatrix} C = \begin{bmatrix} w_0 \\ \vdots \\ w_{k-1} \end{bmatrix}. \tag{1.60}$$

Again, for k small, there are multiple solutions. We next restrict C to be a linear combination of k basis functions. Let $\{\phi_j\}$ be a set of basis functions where $\phi_j : \mathbb{R}^d \to \mathbb{R}$, $j = 0, 1, 2, \ldots, n-1$, such as Hermite polynomials. Define the matrix consisting of these basis functions as column vectors:

$$\Phi := [\phi_0, \phi_1, \ldots, \phi_{n-1}] \in \mathbb{R}^{m \times n}. \tag{1.61}$$

We rewrite (1.54) in terms of these basis functions. For each i, j take

$$A_{ij} = \Phi\alpha_{ij}, \quad \alpha_{ij} \in \mathbb{R}^n, \tag{1.62}$$

$$B_i = \Phi\beta_i, \quad \beta_i \in \mathbb{R}^n, \tag{1.63}$$

and

$$\alpha := \begin{bmatrix} \alpha_{11} \\ \vdots \\ \alpha_{ij} \\ \vdots \\ \alpha_{dd} \end{bmatrix} \in \mathbb{R}^{nd^2}, \quad \beta := \begin{bmatrix} \beta_1 \\ \vdots \\ \beta_j \\ \vdots \\ \beta_d \end{bmatrix} \in \mathbb{R}^{nd},$$

$$c := \begin{bmatrix} \alpha \\ \beta \end{bmatrix} \in \mathbb{R}^{(nd^2+nd)}. \tag{1.64}$$

As in (1.51-1.53), define the differential operators restricted to these basis functions:

$$D^2_\Phi(U) := [D^2_{11}U\Phi, \ldots, D^2_{ij}U\Phi, \ldots, D^2_{dd}U\Phi] \in \mathbb{R}^{m \times nd^2} \tag{1.65}$$

$$D^1_\Phi(U) := [D_1U\Phi, \ldots, D_iU\Phi, \ldots, D_dU\Phi] \in \mathbb{R}^{m \times nd} \tag{1.66}$$

$$D_\Phi(U) := [D^2_\Phi(U), D^1_\Phi(U)] \in \mathbb{R}^{m \times (nd^2+nd)}. \tag{1.67}$$

Rewrite equation (1.60) as

$$D_{\Phi,k}c := \begin{bmatrix} D_\Phi(V_0) \\ \vdots \\ D_\Phi(V_{k-1}) \end{bmatrix} c = \begin{bmatrix} w_0 \\ \vdots \\ w_{k-1} \end{bmatrix} := W_k, \tag{1.68}$$

where $D_{\Phi,k} \in \mathbb{R}^{km \times (nd^2+nd)}$, $c \in \mathbb{R}^{(nd^2+nd)}$, $W_k \in \mathbb{R}^{km}$.

We solve for c through least squares:

$$\min_c \left[D_{\Phi,k}c - W_k\right]^* \left[D_{\Phi,k}c - W_k\right], \tag{1.69}$$

which results in

$$c = \left[D^*_{\Phi,k}D_{\Phi,k}\right]^{-1} D^*_{\Phi,k}W_k. \tag{1.70}$$

We would like to compare the eigenfunctions of the approximated model with the eigenfunctions appearing in equation (1.57). We compute the approximate Markov matrix:

$$\hat{D}(c) := \sum_{i,j=1}^{d} D^2_{ij}\text{diag}\{\Phi\alpha_{ij}\} + \sum_{i=1}^{d} D^1_{ij}\text{diag}\{\Phi\beta_i\}. \tag{1.71}$$

The approximate Markov matrix is then

$$\hat{P} = I + \delta t\hat{D}(c). \tag{1.72}$$

We then compare the spectrum of $\hat{D}(c)$ with the spectrum in (1.57).

Application Example

In this section, we construct a reduced order model describing nonlinear oscillations of flame dynamics. High-speed video data was obtained from the UTRC combustion rig described in [73], and proper orthogonal decomposition (POD) was used for dimension-reduction. We briefly describe how the Markov matrix was empirically constructed.

Data Reduction using POD Modes

From the image data, the mean field was removed from each of the images and the POD modes were computed. It was found that the first two POD modes account for more than 80% of the energy found in the data set. Hence, we consider a two dimensional state space $x \in \mathbb{R}^2$. The two-dimensional time series is constructed via

$$x_k = \begin{bmatrix} x_{1,k} \\ x_{2,k} \end{bmatrix} = \begin{bmatrix} \langle \phi_1, \tilde{y}_k \rangle \\ \langle \phi_2, \tilde{y}_k \rangle \end{bmatrix} \tag{1.73}$$

where $\tilde{y}_k$ denotes the k-th image with the mean field subtracted.

The time series of POD coefficients, given by $\{x_k\}$, were obtained from projecting the original data onto the POD modes. The resulting phase space (plotting $x_{1,k}$ vs. $x_{2,k}$, for $k = 1, \ldots, N$) is shown in figure (1.1). The phase portrait shows a noisy limit cycle where the density of points is clearly non-uniform. The rotational speed of the limit-cycle varies depending on the state. This indicates that a nonlinear model is necessary to match this time series.

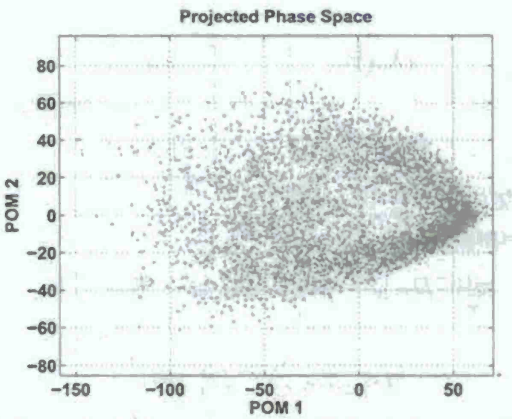

Figure 1.1: The phase space of the coefficients resulting from projection of the data onto the first two POD modes

Empirical Markov Model

A Markov model was computed from this time series data through equation (1.45). The result is a non-reversible Markov model with many eigenvalues, as shown in Figure 1.2. Note that the eigenvalues can be collapsed toward the origin by taking powers of P. The eigenvector corresponding to the unit eigenvalue, shown in Figure 1.3 confirms the steady distribution of the trajectories.

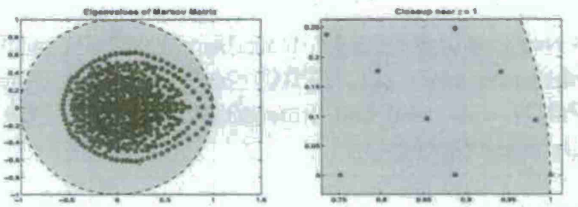

Figure 1.2: The eigenvalues of the Markov model.

The phase of the eigenvector associated with the 2nd eigenvalue is shown in Figure 1.4. It reveals the oscillatory nature of the dynamics.

Nonlinear Model Extraction

In this section we develop a second order stochastic differential equation model of the form

$$\begin{aligned} \dot{x}_1 &= b_1(x_1, x_2) + \sigma_{11}\xi_1 \\ \dot{x}_2 &= b_2(x_1, x_2) + \sigma_{22}\xi_2 \end{aligned} \tag{1.74}$$

to capture the essential dynamical behavior of the reduced set of data from the previous section.

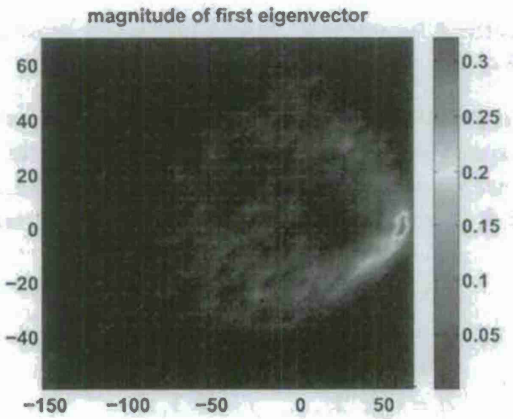

Figure 1.3: The first eigenvector shows the invariant distribution

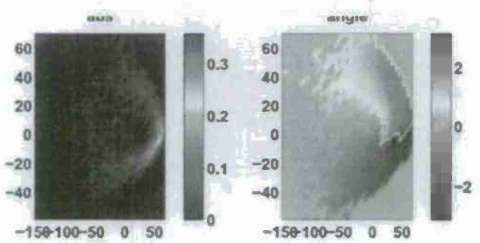

Figure 1.4: Magnitude(left) and phase(right) of the second eigenvector

Before going into the details of the model we would like to summarize some of the key dynamical features of the reduced set of data as captured by phase portrait in Figure 1.1.

- Dynamics consist of stable limit cycle where the motion along the limit cycle is in clockwise direction.
- The limit cycle is parameterized by angle θ. Speed along the limit cycle is nonuniform, speed of the limit cycle is less for $\theta \in [0, -\frac{\pi}{2}]$ compared to other value of θ.

We would like the model to capture this essential dynamical behavior along with the amplitude of the limit cycle and the average speed or the frequency of the limit cycle. We choose a reduced set of eigenvalues closest to the unit circle to approximate the Markov model. Due to the cyclic nature of the data, we use basis functions Φ in radial coordinates, expressed as separable functions in r and θ

$$\begin{aligned}
\phi_{k,0}(x_1, x_2) &= r^k \\
\phi_{k,2j}(x_1, x_2) &= r^k \cos(j\theta) \\
\phi_{k,2j+1}(x_1, x_2) &= r^k \sin(j\theta), \\
k = 0, 1, 2, \ldots, \; j &= 0, 1, 2, \ldots
\end{aligned}$$

where

$$\begin{aligned}
x_1 &= r\cos\theta \\
x_2 &= r\sin\theta
\end{aligned}$$

The least squares fit (1.70) resulted in basis function coefficients producing the terms appearing on the right hand side of (1.74). The functions $b_1(x_1, x_2)$ and $b_2(x_1, x_2)$ appear in Figures 1.5 and 1.6, respectively. The resulting functions $\sigma_{11}(x_1, x_2)$ and $\sigma_{22}(x_1, x_2)$ are qualitatively similar.

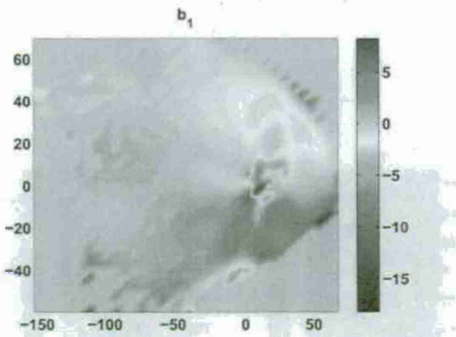

Figure 1.5: The estimated $b_1(x_1, x_2)$ appearing in (1.74).

The resulting approximate eigenfunctions of the estimated Markov matrix are shown in Figure 1.7 and 1.8. Figure 1.7 shows the approximate invariant distribution which closely resembles that shown in Figure 1.3. Similarly, the second complex-valued approximate eigenfunction is shown in Figure 1.8 which closely resembles the second eigenfunction shown in Figure 1.4. The match in the eigenfunction indicates a good match between the model and the data in terms of long term dynamics.

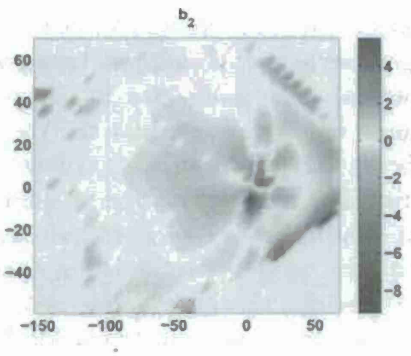

Figure 1.6: The estimated $b_2(x_1, x_2)$ appearing in (1.74).

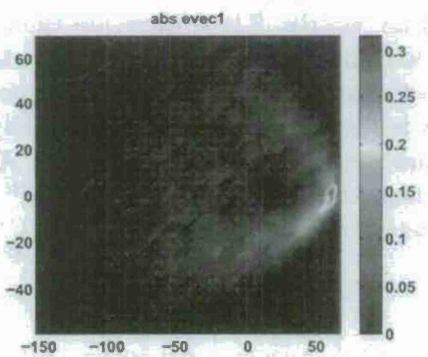

Figure 1.7: The approximate first eigenvector of the estimated Markov matrix

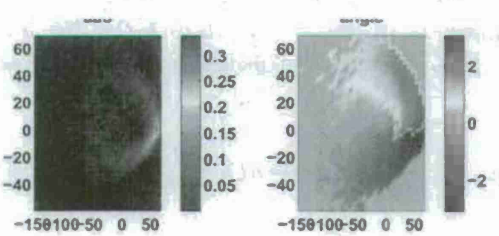

Figure 1.8: The approximate magnitude(left) and phase(right) of the second eigenvector of the estimated Markov matrix

1.1.3 Analysis of Complex Spectra and Metastability

The purpose of this paper is to develop methods for model reduction for diffusion processes that exhibit cyclic behavior. For this purpose we extend techniques based on the spectral theory of Markov processes to the case of complex spectra. The main idea is to augment the state process for the diffusion with a clock process. For each complex eigenvalue for the original diffusion there exists a real eigenvalue for the augmented process. Results concerning metastability (or quasi-stationarity) are then applied to the augmented process. For the special case of a linear diffusion in two dimensions, this is analogous to analyzing the process in a rotating coordinate frame. The results are illustrated through a linear diffusion, and an empirical model of combustion dynamics.

Extensions of the classical Wentzell–Freidlin theory for model reduction have appeared in numerous papers over the past decade. Much of this work has concerned Markov processes that are reversible [59, 21, 13, 37, 14, 15]. The goal in these papers is to understand the statistics of exit times from a given subset of the state space.

Some results for non-reversible Markov chains are available. Fill's paper [29] extends the convergence-rate bound of Diaconnis and Stroock [22] to non-reversible Markov chains. For this purpose the transition matrix is replaced by its symmetrization, and the rate of convergence is bounded by the eigenvalues of the resulting self-adjoint matrix. These ideas are the basis of [38] that establishes exit time statistics from a set for a discrete-time non-reversible Markov chain.

Extensions of Wentzell–Freidlin theory to non-reversible processes appeared for the first time in [38]. The foundation of this paper is the theory of quasi-stationarity, building on the work of [27]. The main idea of [38] can be summarized as follows: Suppose that $\boldsymbol{X} = \{X(t) : t \in \mathbb{T}\}$ is a diffusion process evolving on $\mathsf{X} = \mathbb{R}^d$, with transition semigroup denoted $\{P^t : t \in \mathbb{T}\}$. We say that Λ is an eigenvalue with (non-zero) eigenfunction h if for each t,

$$P^t h = e^{\Lambda t} h$$

Suppose that Λ is real and negative. In this case we can assume that h is also real-valued, and we also assume that it is continuous. We would like to consider *Doob's h-transform*, $\check{P}^t := e^{-\Lambda t} I_h^{-1} P^t I_h$, where I_g is the multiplication operator: For each $x \in \mathsf{X}$ and $A \subset \mathsf{X}$ we have $I_g(x, A) = g(x)\mathbb{I}\{x \in A\}$. The h-transform, like importance-sampling, is intended to lead to a new Markov model whose properties provide insight into the problem of interest. Unfortunately $\{\check{P}^t\}$ is not a valid Markov semigroup since h may take on negative values. Instead we consider the following restricted definition.

Let M denote a connected component of the set $\{x : h(x) > 0\}$. We let $T_\bullet = \inf(t > 0 : Y(t) \in \mathsf{M}^c)$, and for $t \in \mathbb{T}$ denote $t_\bullet = t \wedge T_\bullet$. The *twisted semi-group* is defined for each $t \in \mathbb{T}$, $x \in \mathsf{X}$, and $A \in \mathcal{B}$ (i.e. A Borel measurable) via,

$$\check{P}^t(x, A) := \frac{1}{h(x)} \mathsf{E}_x\big[e^{-\Lambda t_\bullet} h(X(t_\bullet)) \mathbb{I}\{X(t_\bullet) \in A\}\big] \tag{1.75}$$

Under general conditions, it is shown in [38] that the twisted semi-group corresponds to a diffusion process on M that is exponentially ergodic. Exponential ergodicity of the twisted process then implies a form of quasi-stationarity, and from this it follows that the exit time from M is approximately exponentially distributed with parameter $|\Lambda|$.

The inspiration for consideration of the twisted process was the work of [27], and techniques from the large deviations analysis contained in [5, 41].

The main result of this paper is the extension of the results of [38] to the case in which $\Lambda \in \mathbb{C}$ is complex. The main idea is to augment the state process for the diffusion with a clock process. For each complex eigenvalue for the original diffusion there exists a real eigenvalue for the augmented process. Results concerning metastability contained in [38] are then applied to the augmented process.

It is assumed that $\boldsymbol{X} = \{X(t) : t \in \mathbb{T}\}$ is a diffusion process evolving on $\mathsf{X} = \mathbb{R}^d$, with transition semigroup denoted $\{P^t : t \in \mathbb{T}\}$. Letting u denote the drift, and Σ the covariance matrix, the differential generator (see e.g. [45]) is defined for C^1 functions $h\colon \mathsf{X} \to \mathbb{C}$ by $\mathcal{D}h\,(x) :=$

$$\sum_i u_i(x) \frac{d}{dx_i} h\,(x) + \tfrac{1}{2} \sum_{ij} \Sigma_{ij}(x) \frac{d^2}{dx_i dx_j} h\,(x) \tag{1.76}$$

or, in more compact notation,

$$\mathcal{D} = u \cdot \nabla + \tfrac{1}{2} \mathrm{trace}\,(\Sigma \Delta)$$

For each $\beta > 0$ the resolvent kernel is given as the Laplace transform,

$$R_\beta := \int_0^\infty e^{-\beta t} P^t \, dt. \tag{1.77}$$

We write $R := R_\beta$ when $\beta = 1$.

It is assumed as in [38] that the diffusion is *V-uniformly ergodic*: For a probability measure ν on $\mathcal{B}$, some constants $b < \infty$ and $\overline{\Gamma} > 0$, a function $s : \mathsf{X} \to [0, \infty)$, and a $V : \mathsf{X} \to [1, \infty)$:

$$\begin{aligned} \mathcal{D}V &\le -\overline{\Gamma} V + bs \\ R &\ge s \otimes \nu. \end{aligned} \tag{V4}$$

The second inequality in (V4) means that the function s and probability measure ν are *small*. This terminology and the outer product notation are taken from [57]. This 'smallness assumption' is equivalently expressed,

$$R(x, A) \ge s(x)\nu(A), \qquad x \in \mathsf{X},\ A \in \mathcal{B}.$$

Suppose that $\mathcal{D}$ has a complex eigenvalue Λ, which we write as

$$\Lambda = -\Gamma + i\vartheta$$

with $\Gamma > 0$, and $\vartheta \neq 0$, with associated eigenvector h. Consider the clock process defined by,

$$\Phi(t) = \Phi(0) e^{i\vartheta t}, \qquad t \ge 0, \tag{1.78}$$

with initial condition restricted to the unit circle in $\mathbb{C}$, which is denoted U. The clock process is Markov, as is the bivariate process,

$$Y(t) = \begin{pmatrix} X(t) \\ \Phi(t) \end{pmatrix}, \qquad t \ge 0.$$

In fact $\boldsymbol{Y}$ is a diffusion on $\mathsf{Y} = \mathsf{X} \times \mathsf{U}$ whose covariance matrix for y is given by,

$$\Sigma_Y(y) := \operatorname{diag}(\Sigma(x), 0). \tag{1.79}$$

Throughout the paper we adopt the notation $y = (x, \phi)$ for $y \in \mathsf{Y}$, with $x \in \mathsf{X}$, $\phi \in \mathsf{U}$.

We define for each real $\beta \in \mathbb{R}$ the real-valued function,

$$g_\beta(y) = \operatorname{Re}\big((e^{i\beta}/\phi)h(x)\big), \qquad y = (x, \phi) \in \mathsf{Y}. \tag{1.80}$$

Proposition 1.1.1 *For each $\beta \in \mathbb{R}$ the function g_β is an eigenfunction for the process $\boldsymbol{Y}$, with eigenvalue $\Lambda_Y = -\Gamma$.*

Proof. The differential generator for $\boldsymbol{X}$ can be extended in the obvious way to $\boldsymbol{Y}$. Given the simple dynamics of $\boldsymbol{\Phi}$ we have for any function $f\colon \mathsf{U} \to \mathbb{C}$,

$$\mathcal{D}f\,(\phi) = i\vartheta\phi f'(\phi)$$

With $f(\phi) = 1/\phi$ the eigenfunction equation holds,

$$\mathcal{D}f\,(\phi) = -i\vartheta\phi/(\phi)^2 = -i\vartheta f(\phi), \qquad \phi \in \mathsf{U}.$$

Hence the generator applied to g_β gives,

$$\begin{aligned}
\mathcal{D}g_\beta\,(y) &= \operatorname{Re}\big((e^{i\beta}/\phi)\mathcal{D}h\,(x)\big) \\
&\quad + \operatorname{Re}\big(-i\vartheta(e^{i\beta}/\phi)h\,(x)\big) \\
&= \operatorname{Re}\big((e^{i\beta}/\phi)\Lambda h(x) \\
&\quad + -i\vartheta(e^{i\beta}/\phi)h\,(x)\big) \\
&= -\Gamma g_\beta(y), \qquad\qquad y \in \mathsf{Y}.
\end{aligned}$$

■

The twisted process

To define the twisted process we fix $\beta = 0$ in the definition (1.80), and let M denote a connected component of $\{y : g_0(y) > 0\}$. It is assumed that this set has nice topological properties: M is equal to the closure of its interior. Following [38], we define $T_\bullet = \inf(t > 0 : Y(t) \in \mathsf{M}^c)$, and the associated twisted process as follows:

The twisted process is the Markov process $\check{\boldsymbol{Y}}$ with state space M whose semigroup is defined using (1.75) based on the eigenfunction g_0. Equivalently, for each $f \in L_\infty(\mathsf{M})$, and any $x \in \mathsf{M}$,
$\check{P}^s f\,(y) := \check{\mathsf{E}}_y[f(\check{Y}(s))] =$

$$\frac{1}{g_0(y)}\mathsf{E}_y[g_0(Y(s \wedge T_\bullet))f(Y(s \wedge T_\bullet))\exp((s \wedge T_\bullet)\Gamma)]$$

The twisted process has a generator defined for C^2 functions $f\colon \mathsf{Y} \to \mathbb{C}$ by,

$$\check{\mathcal{D}}f = g_0^{-1}\mathcal{D}(g_0 f) + \Gamma f. \tag{1.81}$$

Two key assumptions are imposed in [38]: First, that the diffusion is *hypoelliptic* (which is used to conclude that the resolvent possesses a density with respect to Lebesgue measure). Second, it is assumed that the gradient of the eigenfunction does not vanish on the boundary of M. The gradient assumption is maintained here. To ensure that $\boldsymbol{Y}$ is hypoelliptic we assume that $\boldsymbol{X}$ is *elliptic*, meaning that its covariance is strictly positive. These assumptions are collected together as follows:

$$\Sigma(x) > 0,$$

$$\nabla_x g_0(y) = \mathrm{Re}\,(\phi^{-1}\nabla h\,(x)) \neq 0, \forall y \in \partial\mathsf{M}. \tag{1.82}$$

It is not hard to see that the assumption (1.82) always fails when $\boldsymbol{X}$ is a diffusion in one-dimension. We see in the next section that it does hold in many examples, such as the linear diffusion in two or more dimensions.

The following result is a consequence of Theorem 3.7 of [38]. The reader is referred to this paper for a precise definition of metastability — Its main conceptual conclusion is that the exit time $\tau_\bullet$ is approximately exponentially distributed, and that the process 'almost' reaches a 'local' steady-state prior to exiting M.

Theorem 1.1.2 *Assume that (V4) is also satisfied for a continuous function $V : \mathsf{X} \to [1, \infty)$. Suppose that h is an eigenfunction with complex eigenvalue $\Lambda = -\Gamma + i\vartheta$ satisfying the following conditions:*

(a) $0 < \Gamma < \overline{\Gamma}$.

(b) $g_0(y) > 0$ *for all* $x \in \mathsf{M}$, *and* $g_0(x) = 0$ *for* $x \in \partial\mathsf{M} := \bar{\mathsf{M}} \setminus \mathsf{M}$.

(c) *Condition (1.82) holds. Consequently, for* $y \in \partial\mathsf{M}$, $(\nabla g_0(x))^{\mathsf{T}}\Sigma_Y(y)(\nabla g_0(y)) > 0$.

(d) $K_n := \{x \in \mathsf{X} : V(x) \le n g_0(x)\}$ *is a compact subset of* X *for each* $n \ge 1$.

Then,

(i) *The escape-time from* M *for the twisted process is infinite a.s. for* $\check{Y}(0) = y \in \mathsf{M}$;

(ii) *The twisted process is* $\check{V}_1$*-uniformly ergodic with* $\check{V}_1(y) = V(x)/g_0(y)$, $y \in \mathsf{Y}$.

(iii) *The set* M *is both metastable and* V*-metastable, with exit rate* $\Gamma(\mathsf{M}) = \Gamma_V(\mathsf{M}) = \Gamma$. *In particular,*

$$\mathsf{E}[e^{\varepsilon\tau_\bullet}] \begin{cases} = \infty & \text{if } \varepsilon \ge \Gamma \\ < \infty & \text{otherwise.} \end{cases}$$

□

The proof of Theorem 1.1.2 amounts to establishing a version of (V4) for the twisted process. We can follow the same steps as in [38] to construct the required Lyapunov function.

For a given $0 < \alpha < 1$ write

$$\check{V}_1 := g_0^{-1}V,\ \check{V}_2 := g_0^{-1}g_0^{\alpha}, \quad \text{and } \check{V} := \check{V}_1 + \check{V}_2\,.$$

We denote $G_0 = \log(g_0)$, where g_0 is the eigenfunction for $\boldsymbol{Y}$. From (V4) and the eigenvector equation we have,

$$\begin{aligned}
\check{\mathcal{D}}\check{V}_1 &= [I_{g_0}^{-1}\mathcal{D}I_{g_0} + \Gamma I]g_0^{-1}V \\
&= g_0^{-1}[\mathcal{D}V + \Gamma V] \\
&\leq -(\overline{\Gamma} - \Gamma)\check{V}_1 + bg_0^{-1}s \\
\\
\check{\mathcal{D}}\check{V}_2 &= [I_{g_0}^{-1}\mathcal{D}I_{g_0} + \Gamma I]g_0^{-1+\alpha} \\
&= g_0^{-1}[\mathcal{D}g_0^{\alpha} + \Gamma g_0^{\alpha}] \\
&= \alpha g_0^{\alpha-1}[\Gamma - \tfrac{1}{2}(1-\alpha)\nabla G_0^{\mathcal{T}}\Sigma_Y \nabla G_0].
\end{aligned}$$

Following arguments in [38], we obtain a version of (V4) for the twisted process: For a finite constant b_0, and a compact set $S \subset \mathsf{M}$,

$$\check{\mathcal{D}}\check{V} \leq -\tfrac{1}{2}(\overline{\Gamma} - \Gamma)\check{V} + b_0\mathbb{I}_S.$$

Examples

We discuss an analytic example as well as an example motivated by an empirical model of limit-cycling combustion dynamics.

Ornstein-Uhlenbeck process

Consider the Ornstein-Uhlenbeck process,

$$dX(t) = AX(t)\,dt + dW(t), \tag{1.83}$$

where $\boldsymbol{W}$ is a full-rank Gaussian process. Suppose that Λ is a complex eigenvalue, and v a (non-zero) left-eigenvector for A, satisfying

$$A^{\mathcal{T}}v = \Lambda v.$$

The generator for $\boldsymbol{X}$ shares this eigenvalue, and the function $h(x) = v^{\mathcal{T}}x$ is an eigenfunction:

$$\begin{aligned}
\mathcal{D}h(x) &= (Ax)^{\mathcal{T}}\nabla h(x) + \tfrac{1}{2}\mathrm{trace}\,(\Sigma\Delta h(x)) \\
&= x^{\mathcal{T}}A^{\mathcal{T}}v = \Lambda h(x).
\end{aligned}$$

We now check to see if (1.82) is satisfied. We have,

$$\nabla_x g_0(y) = \mathrm{Re}\,(\phi^{-1}v), \qquad y = (x,\phi) \in \mathsf{Y}.$$

This is zero if and only if $\mathrm{Re}\,(\phi^{-1}v_k) = 0$ for each $k = 1,\dots,n$. If this holds for some $\phi \in \mathsf{U}$, it then follows that $v^* = i\phi^{-1}v$ is a purely real eigenvector for A, which is impossible since Λ is complex. We conclude that (1.82) is satisfied.

Consider the two-dimensional model with

$$A = \begin{bmatrix} -a & 1 \\ -1 & -a \end{bmatrix}$$

where $a > 0$. The matrix A possesses a pair of complex eigenvalues in the left-hand complex plane, satisfying $\Gamma = a$:

$$\text{eig}\,(A) = -a \pm i.$$

A left eigenvector for A is given by $v^T = [-1,\ i]$, which gives

$$\text{Re}\,(e^{-jt}v^T X(t)) = \cos(t)X_1(t) + \sin(t)X_2(t).$$

If $X(0)$ satisfies $\text{Re}\,(v^T X(0)) > 0$, we can expect that $\text{Re}\,(e^{-jt}v^T X(t)) > 0$ for a period of time approximately exponentially distributed, with mean $1/a$. Applying Theorem 1.1.2 we conclude that the first exit time $T_\bullet = \inf(t > 0 : \text{Re}\,(e^{-jt}v^T X(t)) = 0)$ shares the following property with the exponential distribution:

$$\mathsf{E}[e^{\varepsilon T_\bullet}] \begin{cases} = \infty & \text{if } \varepsilon \geq a \\ < \infty & \text{otherwise.} \end{cases}$$

□

Empirical Model of Limit-Cycling Combustion Dynamics

We apply the analysis to a Markov model describing the nonlinear dynamics of limit-cycling combustion oscillations. The data was obtained from an experimental combustion rig described in [73]. The two-dimensional phase space was obtained as in [?] as follows. A POD analysis was done on the temporal flame images and the data was projected on to the first two dominant POD modes. The dynamics of the flame data projected on to this two-dimensional space is shown in Figure 1.1. The phase portrait shows a noisy limit-cycle where the direction of oscillation is in the clockwise direction.

A discrete time Markov model was constructed for the dynamics on this two-dimensional space. The eigenvalues are shown in Figure 1.9. The complex eigenvalues suggest cyclic behavior and a metastability analysis can be done using the corresponding eigenfunctions as described in the previous sections.

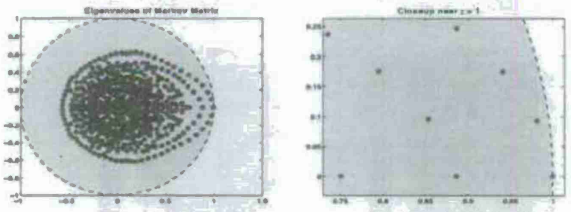

Figure 1.9: Eigenvalues of the Markov matrix associated with the combustion dynamics data shown in Figure ??.

We describe the metastable sets associated with the eigenvalues shown on the right in Figure 1.9. In particular, the eigenvalue at $\lambda := |\lambda|e^{i\psi} = 0.98 + j0.995$ is associated with an eigenfunction that varies in the tangential direction and has no radial variation. The associated eigenvector $h(x)$

is complex as shown in Figure 1.10. We take the clock process to be the discrete time equivalent of (1.78),

$$\phi_k = e^{i\psi k}\phi_0, \qquad k = 1, 2, \ldots,$$

where ψ is the angle of the eigenvalue λ. Setting $\phi_0 = 1$, the eigenfunction of the associated twisted process is

$$g_0(y) = \mathrm{Re}\left(e^{-i\psi k}h(x)\right), \qquad y = (x, \phi) \in \mathsf{Y}.$$

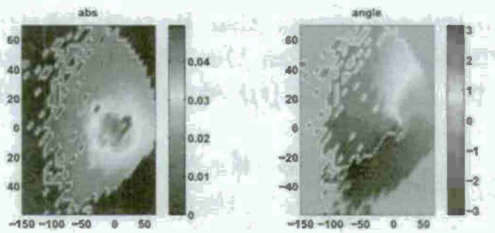

Figure 1.10: The complex eigenvector $h(x)$ (magnitude on right, phase angle on left) associated with the complex eigenvalue $\lambda = 0.98 + j0.995$ shown in Figure 1.9.

The plot in Figure 1.11 shows the sign of $g_0(y)$ for different phase-shifts (i.e, after multiplication by $e^{-i\psi k}$ for different values of k.). Note how the sets with positive support and negative support rotate around the phase space and the exit time marks the point when the system exits one of these rotating sets (i.e., exhibits a phase-shift in its oscillations).

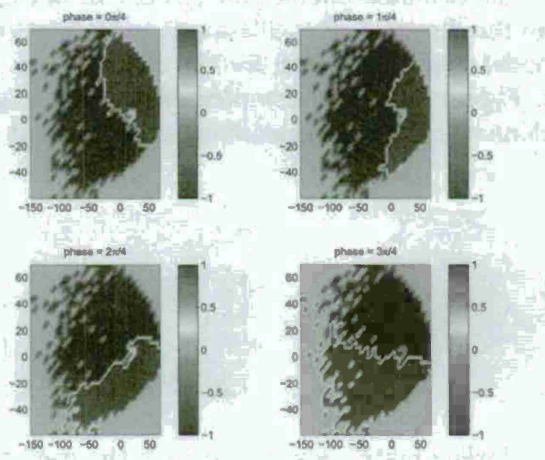

Figure 1.11: The sign of the eigenfunction with a complex eigenvalue close to the unit circle, rotating with incremental phase-shifts of $\frac{\pi}{4}$ between 0 and $\frac{3\pi}{4}$.

The eigenvalue $\lambda = 0.89$ is purely real and hence has a purely real eigenvector with no tangential variation, but variation in the radial direction. The sign of the eigenvector is shown in Figure 1.12.

Since the eigenvalue is real, this eigenvector is not associated to any cyclic behavior. This eigenvector and the related exit time simply indicates when the system moves from a state of low amplitude oscillation to high amplitude oscillation, and vice-versa.

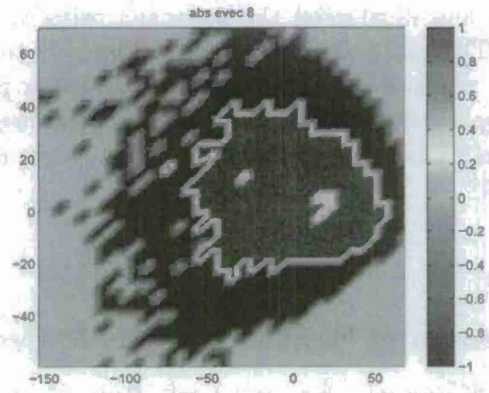

Figure 1.12: The sign of the radial eigenvector of the Markov matrix.

Finally, the complex eigenvalue $\lambda = 0.851 + j0.99$ has an eigenvector exhibiting both tangential and radial components. Note again how the metastable set rotates around the phase-space, as indicated by the phase-shifted sign of the eigenvector shown in Figure 1.13.

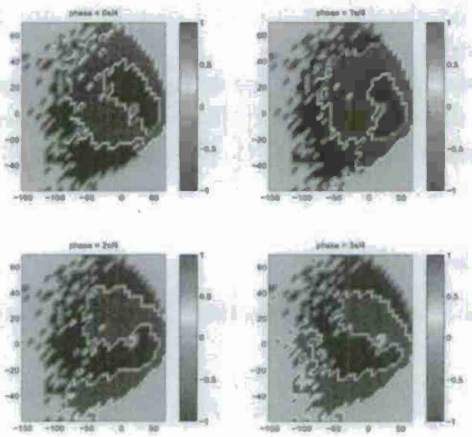

Figure 1.13: The sign of the eigenvector with tangential and radial variation, shown rotating with incremental phase-shifts of $\frac{\pi}{4}$ between 0 and $\frac{3\pi}{4}$.

By examination of the magnitudes of the eigenvalues, the eigenvectors associated with these three metastable sets have decreasing mean exit times. This is intuitively confirmed by the fact that the

sets become increasingly complicated. A hierarchy of such sets along with the spectral properties of the Markov matrix can be used to construct a reduced order model of the measured process through techniques described in [64].

We have presented a framework for analyzing Markov models with semi-rotational dynamics by considering the complex spectra, and illustrated the approach using an application involving limit-cycling combustion oscillations. The ultimate goal of this research is to construct low order models that capture essential structure, such as the hidden Markov models proposed in [38]. The most interesting open problems are application specific. For example, can we justify the consideration of a two-dimensional model obtained from POD coefficients? If not, what are alternative approaches to treat the full-order Markov model?

1.2 Model Reduction

1.2.1 Tangent Space Approach to Nonlinear Model Reduction and Identification

In this section we discuss a novel approach for model reduction of nonlinear systems with output measurements based on the analysis of linear derivative maps [74]. With every nonlinear system one can associate a linear derivative map that evolves vectors on the tangent space. At each point along a nominal trajectory, a local observability gramian defined on the tangent space is computed based on the linear perturbation dynamics, which is then used to identify a balanced local coordinate system. These local coordinates can be patched together to construct the global coordinates for the reduced order representation of the system. A computational approach is described for the empirical construction of the gramian on the tangent space and for the alignment of the local coordinates to obtain the global coordinates. Simulation results and examples are presented to demonstrate the application of the proposed method.

Previous methods of model reduction include, for example, techniques based on proper orthogonal decomposition (POD) for of fluid flows problem [11], [62], balanced truncation in control systems [54], [65], [43], spectral analysis of transfer operators [51], [52], and fast and slow manifold decomposition [30] in dynamical systems.

Derivative Gramian and Model reduction

Consider the model reduction problem for a discrete time dynamical system with output measurement as follows:

$$\begin{aligned} x_{k+1} &= f(x_k) \\ y_k &= h(x_k) \end{aligned} \tag{1.84}$$

where $x \in X \subset \mathbb{R}^n$ is a compact state space and $y \in Y \subset \mathbb{R}^m$. Associated with the nonlinear system is a linear derivative map obtained from the linearization of the system along a nominal trajectory.

The linear derivative map evolves vectors on the tangent space and is defined as follows:

$$\begin{aligned} \eta_{k+1} &= \frac{\partial f}{\partial x}(x_k)\eta_k =: A(x_k)\eta_k \\ \phi_k &= \frac{\partial h}{\partial x}(x_k)\eta_k =: C(x_k)\eta_k \end{aligned} \tag{1.85}$$

where $A(x_k) : T_{x_k}X \to T_{f(x_k)}X$ and $C(x_k) : T_{x_k}X \to T_{h(x_k)}Y$. Important information about the system dynamics can be obtained from the linear derivative map. For example, the Lyapunov exponent, which can be thought of as the generalization of eigenvalues from linear systems to nonlinear systems, are obtained from the linear derivative map. The negative (positive) value of maximum Lyapunov exponent implies exponential convergence (divergence) of nearby system trajectories. Evaluation of the derivative map at the trivial solution is widely used in the local stability analysis of the trivial solution.

Under suitable technical conditions [74], for a given point x on the nominal trajectory the observability gramian

$$\mathcal{Q}(x) = \sum_{k=0}^{\infty} \left(\prod_{j=0}^{k-1} A(x_j) \right)' C'(x_k)C(x_k) \prod_{j=0}^{k-1} A(x_j) \tag{1.86}$$

is well defined. It is easy to check that $\mathcal{Q}(x)$ is positive semi-definite and hence defines a pseudo-metric on the tangent space at x, with $\langle \xi, \eta \rangle_{\mathcal{Q}(x)} = \xi' \mathcal{Q}(x)\eta$, where ξ and η are vectors belonging to T_xX. Furthermore, one can verify that $\mathcal{Q}(x_\ell) = A'(x_\ell)\mathcal{Q}(x_{\ell+1})A(x_\ell) + C'(x_\ell)C(x_\ell)$ where $x_{\ell+1} = f(x_\ell)$, which resembles equation (7) in [42], where Lall and Beck write the Lyapunov inequality for a generalized observability gramian.

Since $\mathcal{Q}(x)$ is positive semidefinite we know that there exists a unitary transformation $U(x)$ as a function of x such that $U'(x)U(x) = I$ and $\Sigma(x) = U(x)\mathcal{Q}(x)U'(x)$ is a diagonal matrix. Now consider the coordinate transformation on the tangent space $\psi = U(x)\eta$, $\eta = U'(x)\psi$ so that $\psi_{k+1} = U(x_{k+1})A(x_k)U'(x_k)\psi_k := \hat{A}(x_k)\psi_k$ and $\phi_k = C(x_k)U'(x_k)\eta_k$. The derivative gramian in the new coordinates can be written as $\hat{\mathcal{Q}}(x_\ell) = \sum_{k=\ell}^{\infty} \hat{\mathcal{A}}'(x_\ell^{k-1})\hat{C}(x_k)'\hat{C}(x_k)\hat{\mathcal{A}}(x_\ell^{k-1})$. Now

$$\begin{aligned} \hat{\mathcal{A}}(x_\ell^{k-1}) &= \hat{A}(x_{k-1})\hat{A}(x_{k-2})\cdots\hat{A}(x_\ell) \\ &= U(x_k)A(x_{k-1})A(x_{k-2})\cdots A(x_\ell)U'(x_\ell) \\ &= U(x_k)\mathcal{A}(x_\ell^{k-1})U'(x_\ell) \end{aligned} \tag{1.87}$$

Hence we have

$$\begin{aligned} \hat{\mathcal{Q}}(x_\ell) &= U(x_\ell)\sum_{k=\ell}^{\infty} \mathcal{A}'(x_\ell^{k-1})C'(x_k)C(x_k)\mathcal{A}(x_\ell^{k-1})U'(x_\ell) \\ &= U(x_\ell)\mathcal{Q}(x_\ell)U'(x_\ell) = \Sigma(x_\ell) \end{aligned}$$

Note that the local coordinate $U(x)$ defined at each point of the tangent space provides a diagonal decomposition of the derivative gramian at each point x. One would like to patch these local coordinate

to construct the global coordinate on the phase space. Here we proceed formally and assume that such global coordinate system exists i.e., $z = T(x)$ such that $\frac{\partial T(x)}{\partial x} = U(x)$. In the next subsection we provide a computational approach for aligning these local coordinates to approximate the global coordinates.

We assume that in the diagonal matrix $\Sigma(x)$ has the following structure.

$$\Sigma = \begin{pmatrix} \Sigma_1 & 0 \\ 0 & \Sigma_2 \end{pmatrix}$$

and that $\Sigma_1 >> \Sigma_2$. Let $z = T(x)$ and we partition the state z based on the partition of its derivative gramian Σ i.e., $z = (z^1, z^2) = (T_1(x), T_2(x)) = T(x)$.

It turns out that the reduced order system with the output measurement

$$\begin{aligned} z^1_{k+1} &= T_1(f(T^{-1}(z^1_k, 0))) \\ \hat{y}_k &= h(T^{-1}(z^1_k, 0)) \end{aligned} \tag{1.88}$$

can be shown to have non-positive Lyapunov exponents with diagonal derivative gramian $\Sigma_1(\hat{z}_k, 0)$.

The computation of the empirical gramians is similar in spirit to [43] and [62] but with a key difference: the formulae in [43] subtract the temporal means from the trajectories, which is not applicable in the current setting. Indeed, for the empricial gramian based on the derivative mapping, we must track the trajectories of the nominal mean states and outputs.

Local Tangent Space Alignment

The global coordinate system T computed from the localized coordinates so that $\frac{\partial T(x)}{\partial x} \approx U(x)$ can be approximated through an alignment procedure. Denote the K-dimensional vector all ones by e_K. We approximate the global coordinates T using the initial condition data points in $\{\mathcal{N}_0 \ldots \mathcal{N}_N\}$ following the procedure of [79]. Further analysis and refinements appear in [78, 76, 46]. Locally, the balancing coordinates are given by the transformation $\Psi_k = U'(x_k)\mathcal{N}_k$. Suppose that there is sufficient overlap between the sets of initial conditions [78] and that there are M distinct initial condition points. Furthermore, suppose that the partition is such that $z_1 \in \mathbf{R}^d$. In other words, the reduced order model will be of dimension d. We now construct the global coordinates τ_k for $k = 1, \ldots, N$. Write $T_k = \left[\tau_k^1, \ldots, \tau_k^K\right]$ and seek to minimize $E_k = T_k\left(I - \frac{1}{K} e_K e_K^T\right) - L_k \Psi_k$ for each k. The alignment matrices L_k can be determined separately by use of the Moore-Penrose pseudo-inverse. The global coordinates T_k are approximated by minimizing

$$\sum_k \|E_k\|_F^2 = \sum_k \|T_k W_k\|_F^2 = \|TSW\|_F^2 = \mathrm{Tr}\left(TSWW^T S^T T^T\right)^{\frac{1}{2}} \tag{1.89}$$

where $T = [\tau_1, \ldots, \tau_M] \in \mathbf{R}^{d \times M}$, $S = [S_1, \ldots, S_N] \in \mathbf{R}^{M \times KN}$ where $S_k \in \mathbf{R}^{M \times K}$ is the 0-1 selector matrix such that $TS_k = T_k$, and $W = \mathrm{diag}\,(W_1, \ldots, W_N)$. We apply the constraint that $TT^T = I$. The rows of T are taken to be the eigenvectors associated with the next smallest 2nd through $d+1$st eigenvalues. The reader is directed to [79] for further details on this computation.

Example: Nonlinear System Reduction

We illustrate the computation of the empirical gramians and the global coordinates. Consider the controlled nonlinear system

$$\begin{aligned} r_{k+1} &= r_k + 0.1\,(R - r_k)\,(1 + \cos(10\theta)) \\ \theta_{k+1} &= \theta_k + \Delta + (u_k - \theta_k) \\ z_{k+1} &= z_k \left(\frac{1}{1 + 0.01\,(1 + \cos(\theta))} \right) \\ u_k &= u_{k-1} + \Delta, \quad u_0 = 0 \\ y_k &= [r_k \cos(\theta_k), r_k \sin(\theta_k), z_k]\,. \end{aligned} \tag{1.90}$$

This system has equilibrium $r_k = R, \quad \theta_k = u_k, \quad z_k = 0$. An example of perturbation and nominal trajectories with $\Delta = \frac{2\pi}{100}$ are shown in figure 1.14. Notice that the z-coordinate, while small relative to the radius of $R = 1$, decays slowly.

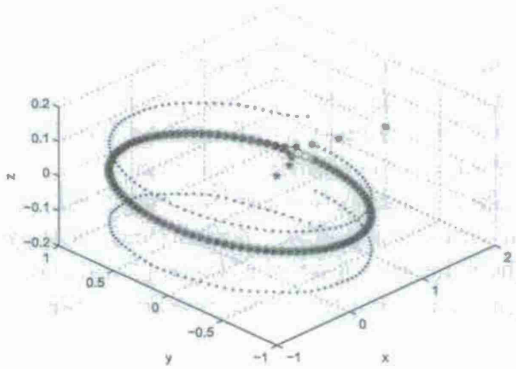

Figure 1.14: Nominal trajectory shown by red circles and example perturbation trajectories shown by blue dots and stars. Initial perturbations are in the $+/-z$ (dots) and $+/-r$ (stars) directions.

A set of initial conditions shown in figure 1.15 (left) was used to compute the empirical derivative gramians and the global balancing coordinate system. Locally, there are two dominant singular values of the gramians, based on the simulation results. The resulting principle component vectors (scaled by the singular values of the gramian) associated with four points are shown in figure 1.15 (right). The vectors show that there are two dominant component directions in the θ, z plane. Although, geometrically the z-coordinate is small compared to the θ coordinate and about equal to the r component, it is dynamically more important because it decays slowly.

The principle components give only local information about the vector field. We employ the alignment procedure described in section 1.2.1 to approximate the global coordinates T. Although we have previously discussed the local principle components associated with the derivative dynamics in terms of the global coordinate system, the alignment procedure requires no a priori information regarding

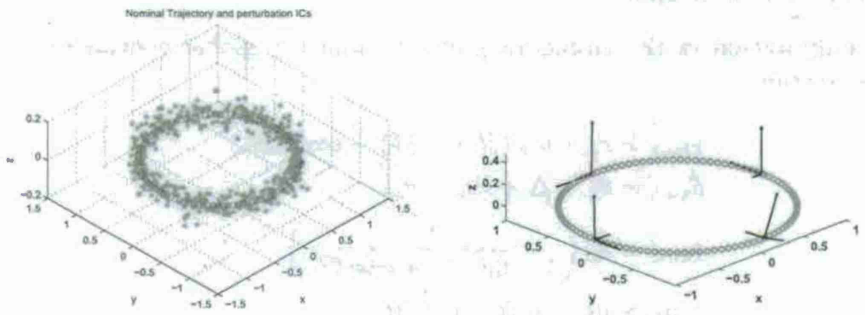

(a) Nominal Trajectory (b) Principal Components

Figure 1.15: Left: Nominal trajectory shown by red circles and the set of initial conditions used to compute the empirical gramians. Right: Local principle component directions computed at four different points on the nominal trajectory.

the global structure of the principle directions. Figure 1.16 (left) shows the resulting approximation of the θ coordinate based on the global alignment of local principle component direction. The figure shows (with the appropriate phase shift) almost a 1-1 relation between the empirically determined global coordinate and the actual θ value of the initial condition.

Figure 1.16 (right) shows a similar relation between the empirically determined z coordinate and the actual z values of the initial condition points. Again (with scaling of -1) there is a near 1-1 correspondence. This example illustrates that a set of reduced global coordinates can be approximated from the local gramian information, with no a priori information regarding the underlying coordinate system of the dynamic model.

Extensions to Dynamic Texture Models

The tangent space approximation in terms of local PCA and the computations of the empirical observability gramian provides a framework for calibrating hybrid affine or nonlinear dynamic texture models, which is the subject of ongoing work at UTRC currently funded by AFOSR. Following the methodology for identifying balanced stochastic systems in [3] we can use the tools described in this section to identify generalizations to the dynamic texture models originally presented in [23]. Such generalizations are appropriate for video data that exhibits nonlinear behavior or mode switching which can be modeled by a piecewise affine [61] dynamic texture. This is similar in spirit to the identification methods based on statistical clustering appearing in [28, 56]. Based on the local PCA representation of the data, locally affine models can be calibrated based on standard L_2 techniques [49]. The model switching is determined by relative distances between the model's current state and the local means of neighboring data patches. The concept of nonlinear dynamic textures has appeared in [48, 4, 47, 77]. An example of a piecewise affine dynamic texture model of the beach video sequence [4] is shown in Figure 1.17 (bottom row), where it is compared with a linear dynamic texture model

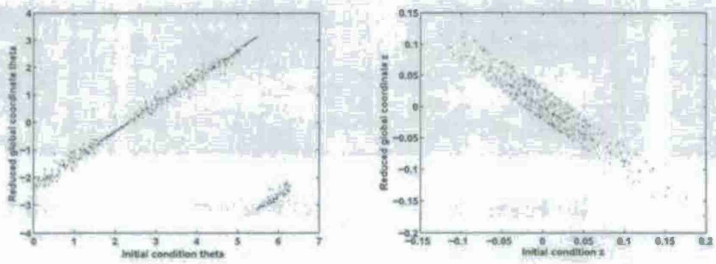

(a) θ coordinates (b) z coordinates

Figure 1.16: Left:The θ component of the estimated global coordinates T compared to the θ components of the initial condition sets $\mathcal{N}_0, \ldots, \mathcal{N}_N$. Right: The z component of the estimated global coordinates T compared to the z components of the initial condition sets $\mathcal{N}_0, \ldots, \mathcal{N}_N$.

(top row). The top row shows that the frames of the linear dynamic texture model capture the bulk motions of the waves and eventually saturate. The piecewise affine model frames shown in the bottom row capture the different dynamic modes of the waves coming inward and outward at the same time increasing the image quality and avoiding saturation effects.

1.2.2 Empirical Controllability Gramians from Trajectories

In this section we provide more details on the computation of empirical gramians.

Suppose that for the controlled system we have the nominal and perturbation trajectories $\{x_k\}$ and $\{\eta_k\}$, respectively, resulting from a nominal control input $\{u_k\}$ and an impulse input v^1. We can write the state history in terms of the impulse input at $k = 0$

$$\begin{bmatrix} \eta^0_{1,1} \\ \eta^0_{2,1} \\ \eta^0_{3,1} \\ \vdots \end{bmatrix} = \begin{bmatrix} B(x_0)v^1 \\ A(x_1)B(x_0)v^1 \\ A(x_2)A(x_1)B(x_0)v^1 \\ \vdots \end{bmatrix}. \tag{1.91}$$

The empirical controllability gramian can be computed from a collection of impulse responses. If we apply the unit impulse v^1 at $k = -j$ then the response is

$$\begin{bmatrix} \eta^{-j}_{-j+1,1} \\ \eta^{-j}_{-j+2,1} \\ \eta^{-j}_{-j+3,1} \\ \vdots \end{bmatrix} = \begin{bmatrix} B(x_{-j})v^1 \\ A(x_{-j+1})B(x_{-j})v^1 \\ A(x_{-j+2})A(x_{-j+1})B(x_{-j})v^1 \\ \vdots \end{bmatrix} \tag{1.92}$$

(a) Frame 20 (b) Frame 40 (c) Frame 60 (d) Frame 80

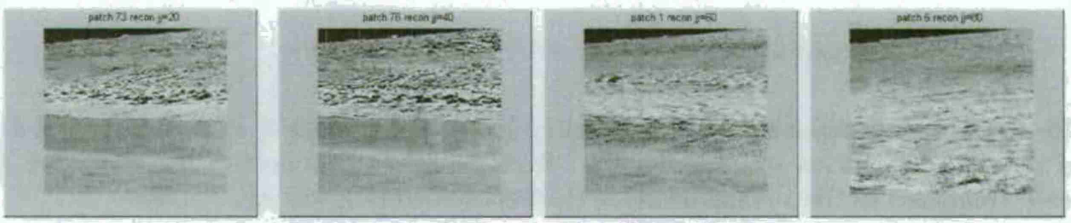

(e) Frame 20 (f) Frame 40 (g) Frame 60 (h) Frame 80

Figure 1.17: Top Row: Linear dynamic texture of beach sequence. Bottom Row: Hybrid affine dynamic texture of beach sequence.

so that

$$\begin{bmatrix} \eta_{1,1}^{-j} \\ \eta_{2,1}^{-j} \\ \eta_{3,1}^{-j} \\ \vdots \end{bmatrix} = \begin{bmatrix} A(x_0)\dots A(x_{-j})B(x_{-j})v^1 \\ A(x_1)\dots A(x_{-j})B(x_{-j})v^1 \\ A(x_2)\dots A(x_{-j})B(x_{-j})v^1 \\ \vdots \end{bmatrix}. \tag{1.93}$$

Suppose we assemble a collection of impulse inputs

$$\mathcal{V} := [\ v^1,\ \dots,\ v^N\ ] \tag{1.94}$$

and their corresponding state responses if the impulse inputs were applied at $k = -j$

$$\mathcal{N}(x_{-j}) = \begin{bmatrix} A(x_0)\dots A(x_{-j})B(x_{-j}) \\ A(x_1)\dots A(x_{-j})B(x_{-j}) \\ A(x_2)\dots A(x_{-j})B(x_{-j}) \\ \vdots \end{bmatrix} \mathcal{V}, \tag{1.95}$$

where the $\mathcal{N}(x_{-j})_{m,\ell} = \eta_{m,\ell}^{-j}$ is the state response at time m with respect to unit impulse input v^ℓ applied at time $k = -j$. Denote the m-th block row of $\mathcal{N}(x_{-j})$ by $\mathcal{N}(x_{-j})_m$. Assume that $\mathcal{V}$ is

orthonormal.

$$\sum_{j=0}^{\infty} \mathcal{N}(x_{-j})_1 \mathcal{N}'(x_{-j})_1 = B(x_0)\mathcal{V}\mathcal{V}'B'(x_0) + A(x_0)B(x_{-1})\mathcal{V}\mathcal{V}'B'(x_{-1})A'(x_0) \tag{1.96}$$

$$+ A(x_0)A(x_{-1})B(x_{-2})\mathcal{V}\mathcal{V}'B'(x_{-2})A'(x_{-1})A'(x_0) + \dots$$

$$= B(x_0)B'(x_0) + A(x_0)B(x_{-1})B'(x_{-1})A'(x_0) \tag{1.97}$$

$$+ A(x_0)A(x_{-1})B(x_{-2})B'(x_{-2})A'(x_{-1})A'(x_0) + \dots$$

$$= \mathcal{B}(x_0)\mathcal{B}'(x_0) = \mathcal{P}(x_1). \tag{1.98}$$

In general the controllability gramian $\mathcal{P}(x_m)$ can be computed

$$\mathcal{P}(x_m) = \sum_{j=-m+1}^{\infty} \mathcal{N}(x_{-j})_m \mathcal{N}'(x_{-j})_m. \tag{1.99}$$

Equation (1.100) can be further averaged as in [43] to include different initial condition matrices and different scalings of the initial conditions. The computation of the empirical controllability gramian is summarized as follows.

Lemma 1.2.1 *Let the matrix $\mathcal{N}(x_{-j})_m$ be the state responses at time index m resulting from the collection of impulse inputs $\mathcal{V}$ applied at time index $-j$, where the ℓ-th column of $\mathcal{N}(x_{-j})_m$ corresponds with the ℓ-th column of $\mathcal{V}$. Then the empirical controllability gramian at x_m is*

$$\mathcal{P}(x_m) = \sum_{j=-m+1}^{\infty} \mathcal{N}(x_{-j})_m \mathcal{N}'(x_{-j})_m. \tag{1.100}$$

■

Note that for any j and m, from (1.95),

$$\mathcal{N}(x_{-j})_{m+1} = A(x_m)A(x_{m-1})\dots A(x_{-j})B(x_{-j}) = A(x_m)\mathcal{N}(x_{-j})_m \tag{1.101}$$

Corollary 1.2.2 *The empirical controllability gramian can be determined by the iteratively through the Lyapunov equation*

$$\mathcal{P}(x_{m+1}) = \mathcal{N}(x_m)_{m+1}\mathcal{N}'(x_m)_{m+1} + A(x_m)\mathcal{P}(x_m)A'(x_m) \tag{1.102}$$

Proof. We have from (1.101)

$$\mathcal{P}(x_{m+1}) = \sum_{j=-m}^{\infty} \mathcal{N}(x_{-j})_{m+1}\mathcal{N}'(x_{-j})_{m+1}$$

$$= \mathcal{N}(x_{m+1})_m \mathcal{N}'(x_{m+1})_m + A(x_m) \sum_{j=-m+1}^{\infty} \mathcal{N}(x_{-j})_{m+1}\mathcal{N}'(x_{-j})_{m+1}A'(x_m)$$

$$= \mathcal{N}(x_m)_{m+1}\mathcal{N}'(x_m)_{m+1} + A(x_m)\mathcal{P}(x_m)A'(x_m) \tag{1.103}$$

■

Of course, the first term in (1.103) is $\mathcal{N}(x_m)_{m+1}\mathcal{N}'(x_m)_{m+1} = B(x_m)B'(x_m)$, so Corollary 1.2.2 states that the empirical gramian can be computed by simulating the previous data an additional time step and adding the state responses from a single-step simulation.

Reverse-Time Adjoint System

As a side note, an alternative formulation of the empirical controllability gramian can be obtained by simulating the reverse-time adjoint system

$$\gamma_{k-1} = A'(\overline{x_k})\gamma_k, \tag{1.104}$$

$$\varphi_k = B'(\overline{x_k})\gamma_k, \tag{1.105}$$

with a series of non-zero initial conditions, as in the empirical observability gramian.

Computations for Empirical Gramians

Computation of the empirical gramians is similar in spirit to [43] and [62] with some key differences. First, the formulae in [43] subtract the temporal means from the trajectories, which is not applicable in the current setting. Indeed, in the current setting we must track the trajectories of the nominal mean states and outputs. Secondly, the Lemma 5 in [43] has the implicit assumption of time-invariance, as does [62].

Perturbation Trajectories

Consider the simulation of the system (1.84) with a fixed control input $\{\overline{u}_k\}$ with a set of N initial conditions $\{x_0^j\}_{j=1_N}$ with average x_0. We have, for the nominal trajectory and for each $j = 1, \ldots, N$

$$x_{k+1} = f(x_k) + g(\overline{u}_k), \;\; y_k = h(x_k) \tag{1.106}$$

$$x_{k+1}^j = f(x_k^j) + g(\overline{u}_k), \;\; y_k^j = h(x_k^j). \tag{1.107}$$

Let $\overline{u_k}$ be a nominal control input and let $\overline{x_k}, \overline{y_k}$ be the resulting response of the state and output, respectively. We consider the system with either a small perturbation on the initial condition η_0^j or a small perturbation on the control v_k and the corresponding state and output perturbations η_k and ϕ_k, respectively. Using the first order terms of a Taylor expansion results in

$$\eta_{k+1} = \frac{\partial f(\overline{x_k})}{\partial x}\eta_k + \frac{\partial b(\overline{u_k})}{\partial u}v_k := A(\overline{x_k})\eta_k + B(\overline{u_k})v_k, \tag{1.108}$$

$$\phi_k = \frac{\partial h(\overline{x_k})}{\partial x}\eta_k := C(\overline{x_k})\eta_k. \tag{1.109}$$

Generalized Gramians

Generalized gramians appear in [9, 34] and are characterized by the Lyapunov inequalities [42]

$$\mathcal{P}(x_k) > B(x_{k-1})B'(x_{k-1}) + A(x_{k-1})\mathcal{P}(x_{k-1})A'(x_{k-1}), \tag{1.110}$$

$$\mathcal{Q}(x_{k-1}) > A'(x_{k-1})\mathcal{Q}(x_k)A(x_{k-1}) + C'(x_{k-1})C(x_{k-1}). \tag{1.111}$$

Existence of solutions appears in [25].

The empirical generalized gramians can be computed iteratively through the time indices: forward in time for the controllability gramians (see Corollary 1.2.2) and backward in time for the observability gramians.

The idea here is to use a single set of initial conditions and check that the matrices of the resulting state responses remains invertible, so it can be used for the computation of the observability gramian at the next time step. This way, we can apply the Lyapunov inequality to the empirical gramians to establish that they are generalized gramians.

Periodic Systems

For periodic system, the iterative construction of the empirical gramians must be modified due to the periodic structure of the system matrices. Consider the controllability gramian of a periodic system with period N so that $\mathcal{P}(x_k) = \mathcal{P}(x_{k+N})$.

Suppose we have computed a nominal empirical gramian $\tilde{\mathcal{P}}(x_0)$ and we apply the following iterative assignments for $k = 0 \dots N-1$. Given $\tilde{\mathcal{P}}(x_k)$ and $\varepsilon_{k+1} > 0$ we compute

$$\tilde{\mathcal{P}}(x_{k+1}) := B(x_k)B'(x_k) + A(x_k)\tilde{\mathcal{P}}(x_k)A'(x_k) + \varepsilon_{k+1} \tag{1.112}$$

$$> B(x_k)B'(x_k) + A(x_k)\tilde{\mathcal{P}}(x_k)A'(x_k). \tag{1.113}$$

Clearly the iterative assignment satisfies the Lyapunov inequality (1.110) for $k = 0 \dots N-1$ but not necessarily for $k = N$ because in general $\tilde{\mathcal{P}}(x_N) \neq \tilde{\mathcal{P}}(x_0)$. We determine scaling factors m_k such that $\mathcal{P}(x_k) = m_k\tilde{\mathcal{P}}(x_k)$ satisfies (1.110) for all $k = 0 \dots N$.

We first state two useful facts regarding scaling.

Lemma 1.2.3 *If $P > 0$ and $P > TPT'$ then for any matrix $R > 0$, there exists a positive constant m such that*

$$mP > mTPT' + R. \tag{1.114}$$

Proof. The result follows by dividing (1.114) by m and applying $m \to \infty$ and $P > TPT'$. ∎

Lemma 1.2.4 *If $P_1 > 0$ $P_2 > 0$ and $P_2 > TP_1T' + R$ with $R > 0$, then if $m_1 > 1$ there exists $m_2 \leq m_1$ such that*

$$m_2P_2 > m_1TP_1T' + R. \tag{1.115}$$

Proof. Take $m_2 = m_1$ to apply $P_2 > TP_1T' + R > TP_1T' + \frac{1}{m_1}R$ to obtain the result. ∎

Finally, repeated application of (1.112) with $\varepsilon_N = 0$ yields

$$\begin{aligned}
\tilde{\mathcal{P}}(x_1) =& B(x_0)B'(x_0) + A(x_0)\tilde{\mathcal{P}}(x_0)A'(x_0) + \varepsilon_1 && (1.116)\\
\tilde{\mathcal{P}}(x_2) =& B(x_1)B'(x_1) + A(x_1)\tilde{\mathcal{P}}(x_1)A'(x_1) + \varepsilon_2\\
=& B(x_1)B'(x_1) + A(x_1)B(x_0)B'(x_0)A'(x_1) + \varepsilon_2 + A(x_1)\varepsilon_1 A'(x_1)\\
&+ A(x_1)A(x_0)\tilde{\mathcal{P}}(x_0)A'(x_0)A'(x_1)\\
&\vdots\\
\tilde{\mathcal{P}}(x_N) =& B(x_{N-1})B'(x_{N-1}) + \cdots + [A(x_{N-1})\ldots A(x_1)]\, B(x_0)B'(x_0)\, [A(x_{N-1})\ldots A(x_1)]'\\
&+ A(x_{N-1})\varepsilon_{N-1}A'(x_{N-1}) + \cdots + [A(x_{N-1})\ldots A(x_1)]\, \varepsilon_1\, [A(x_{N-1})\ldots A(x_1)]'\\
&+ [A(x_{N-1})\ldots A(x_0)]\, \tilde{\mathcal{P}}(x_0)\, [A(x_{N-1})\ldots A(x_0)]' && (1.117)\\
:=& R + T\tilde{\mathcal{P}}(x_0)T', && (1.118)
\end{aligned}$$

where

$$\begin{aligned}
R :=& B(x_{N-1})B'(x_{N-1}) + \cdots + [A(x_{N-1})\ldots A(x_1)]\, B(x_0)B'(x_0)\, [A(x_{N-1})\ldots A(x_1)]'\\
&+ A(x_{N-1})\varepsilon_{N-1}A'(x_{N-1}) + \cdots + [A(x_{N-1})\ldots A(x_1)]\, \varepsilon_1\, [A(x_{N-1})\ldots A(x_1)]' && (1.119)\\
T :=& [A(x_{N-1})\ldots A(x_0)]\,. && (1.120)
\end{aligned}$$

Proposition 1.2.5 *For the N-periodic system, given $\tilde{\mathcal{P}}(x_0)$ and $\{\tilde{\mathcal{P}}(x_k)\}_{k=1,\ldots,N}$ specified by (1.110), there exist positive constants $\{m_k\}_{k=0,\ldots,N}$ such that $\{\mathcal{P}(x_k) := m_k\tilde{\mathcal{P}}(x_k)\}_{k=0,\ldots,N-1}$ satisfy (1.110) for all $k = 0,\ldots,N$ and thus form the matrix blocks of a block-diagonal generalized controllability gramian for the periodic system.*

Proof. The proof is by construction. If $\tilde{\mathcal{P}}(x_0) > \tilde{\mathcal{P}}(x_N)$ then take $m_k = 1, \forall k = 1,\ldots,N-1$. Suppose $\tilde{\mathcal{P}}(x_0) \leq \tilde{\mathcal{P}}(x_N)$. Since the nonlinear system has Lyapunov exponents with magnitudes strictly less than unity, $\tilde{\mathcal{P}}(x_0) > T\tilde{\mathcal{P}}(x_0)T'$. By Lemma 1.2.3, determine m_0 such that

$$m_0\tilde{\mathcal{P}}(x_0) > R + Tm_0\tilde{\mathcal{P}}(x_0)T'. \tag{1.121}$$

Apply Lemma 1.2.4 to equations (1.116-1.117) to determine $\{m_k\}_{k=1,\ldots,N-1}$ with $m_{k+1} \leq m_k \leq m_0$ such that (1.110) holds for $k = 0,\ldots,N-1$. A final application of (1.121) with $\mathcal{P}(x_N) := m_0\tilde{\mathcal{P}}(x_0) = \mathcal{P}(x_0)$ results in

$$\begin{aligned}
\mathcal{P}(x_N) := m_0\tilde{\mathcal{P}}(x_0) &> R + Tm_0\tilde{\mathcal{P}}(x_0)T'\\
&= B(x_{N-1})B'(x_{N-1}) + A(x_{N-1})\mathcal{P}(x_{N-1})A'(x_{N-1}), && (1.122)
\end{aligned}$$

which is just (1.110) with $k = N$. ∎

Corollary 1.2.6 *For the N-periodic system, given $\tilde{\mathcal{Q}}(x_N)$ and $\{\tilde{\mathcal{Q}}(x_k)\}_{k=0,\ldots,N-1}$ specified by (1.111), there exist positive constants $\{q_k\}_{k=0,\ldots,N}$ such that $\{\mathcal{Q}(x_k) := q_k\tilde{\mathcal{Q}}(x_k)\}_{k=1,\ldots,N}$ satisfy (1.111) for all $k = 0,\ldots,N$ and thus form the matrix blocks of a block-diagonal generalized observability gramian for the periodic system.*

1.3 Stability Analysis of Systems with Symmetry-Breaking

1.3.1 Absolute Stability of Coupled Dissipative Parabolic Equations with Wave-Speed Mistuning

Recent work has focussed on the stabilizing properties of symmetry-breaking in oscillator systems. We consider the problem of achieving global absolute stability of an unstable equilibrium solution of coupled dissipative parabolic equations with non-homogeneous coefficients. In particular, we consider the stabilization of a PDE model describing thermo-acoustic instabilities with wave-speed mistuning. Sufficient conditions for absolute stability of the infinite-dimensional system are established by the feasibility of two finite-dimensional linear matrix inequalities (LMI). Numerical results are presented for an example problem.

We establish conditions for absolute stability of the nominally unstable zero solution of a coupled parabolic equation. In particular we are interested in the stabilizing effects of wave-speed mistuning on thermo-acoustic systems with skew-symmetric nonlinear coupling. Some analysis of the finite-dimensional truncation of this system has appeared in [33, 71, 26] and the results have been demonstrated in an actual engine [17]. In most combustion dynamic applications, identifying the exact form of the heat-release coupling is difficult, and therefore it is appropriate to study the absolute stability properties of such systems, where the skew-symmetric feedback is characterized by a sector bound. Recent work has revealed the importance of skew-symmetric coupling in wave-equation systems [7, 8] and how mistuning can enhance the stability of such systems. This phenomena is also common in suppression of blade flutter instabilities [10, 60, 58, 70]. Additionally, recent work has focussed on analysis of heterogeneous distributed systems [24],[40].

Through Lyapunov analysis we establish sufficient conditions for absolute stability by the feasibility of a set of finite-dimensional linear matrix inequalities (LMI) [31, 32]. This paper is organized as follows. In section 1.3.1 we describe the model of thermo-acoustic instabilities with wave-speed mistuning. This model serves as a motivating example to consider more general systems that have off-diagonal linear coupling which is described in section 1.3.1. Stability analysis of the nonlinear infinite-dimensional system is presented in section 1.3.1. In section 1.3.1, a finite number of LMI feasibility conditions are presented that are sufficient for infinite-dimensional absolute stability and the relation with finite-dimensional model truncation is presented in section 1.3.1. A numerical example is shown in section 1.3.1.

Thermo-acoustic Model with Mistuning

We consider the following system that describes rotating thermo-acoustic instabilities as described in [33, 26], with mistuning parameter $a^2(\theta)$ that serves to couple different modes [7, 50].

$$\frac{\partial u}{\partial t} = -a^2(\theta)\frac{\partial p}{\partial \theta} + \nu \frac{\partial^2}{\partial \theta^2} u \tag{1.123}$$

$$\frac{\partial p}{\partial t} = -\frac{\partial u}{\partial \theta} + \xi \frac{\partial^2}{\partial \theta^2} p + Ku + g(u), \tag{1.124}$$

for $\theta \in [0, 2\pi)$ with periodic boundary conditions. In (1.123,1.124) u denotes the transverse acoustic velocity, p denotes the acoustic pressure, $a^2(\theta)$ denotes the acoustic wave-speed, ν and ξ represent vis-

cous and acoustic damping, respectively, and K and $g(\cdot)$ denote, respectively, the linear and nonlinear components of the heat-release coupling (see e.g. [55, 18]). Define the state space

$$x = \begin{bmatrix} u \\ p \end{bmatrix}. \tag{1.125}$$

It is convenient to cast (1.123,1.124) as an evolution equation, so we define the operators

$$\mathcal{A} = \begin{bmatrix} \nu\frac{\partial^2}{\partial\theta^2} & -a^2\frac{\partial}{\partial\theta} \\ -\frac{\partial}{\partial\theta} + K & \xi\frac{\partial^2}{\partial\theta^2} \end{bmatrix}, \mathcal{B} = \begin{bmatrix} 0 \\ 1 \end{bmatrix}, \mathcal{C} = \begin{bmatrix} 1 & 0 \end{bmatrix}, \tag{1.126}$$

so (1.123,1.124) become

$$\frac{\partial}{\partial t}x = \mathcal{A}x + \mathcal{B}g(\mathcal{C}x). \tag{1.127}$$

We now define some finite-dimensional matrices and vectors that will be used in the infinite-dimensional stability analysis. We will use $\{\sin, \cos\}$ basis functions and denote the k-th basis function as

$$\phi_k(\theta) := \frac{1}{\sqrt{\pi}} \begin{bmatrix} \sin(k\theta) & 0 & \cos(k\theta) & 0 \\ 0 & \cos(k\theta) & 0 & \sin(k\theta) \end{bmatrix} \tag{1.128}$$

and the k-th state vector is

$$x_k := \langle \phi_k, x \rangle = \int_0^{2\pi} \phi_k^T(\theta) x(\theta)\, d\theta \tag{1.129}$$

Here the superscripts $[\cdot]^s, [\cdot]^c$ denote the sin and cos components, respectively. As in [26, 50] we consider the mistuned wave-speed of the form

$$a^2(\theta) = a_0^2 + a_2^2 \cos(2\theta). \tag{1.130}$$

For $k = 1$ the finite-dimensional projection of $\mathcal{A}$ is

$$A_1 := \langle \phi_1, \mathcal{A}\phi_1 \rangle = \begin{bmatrix} -\nu & a_0^2 - a_2^2 & 0 & 0 \\ -1 & -\xi & K & 0 \\ 0 & 0 & -\nu & -a_0^2 - a_2^2 \\ K & 0 & 1 & -\xi \end{bmatrix}. \tag{1.131}$$

For $k > 1$ define the matrix $A_k \in \mathbb{R}^{4\times 4}$ such that

$$A_k := \langle \phi_k, \mathcal{A}\phi_k \rangle = \begin{bmatrix} -k^2\nu & ka_0^2 & 0 & 0 \\ -k & -k^2\xi & K & 0 \\ 0 & 0 & -k^2\nu & -ka_0^2 \\ K & 0 & k & -k^2\xi \end{bmatrix}. \tag{1.132}$$

Analysis of the system truncated to a single pair of modes has appeared in [33, 26], where the mistuning produces beneficial coupling between the first pair of modes [7]. The mistuning also produces coupling

between mode pairs k and $k+2$. For $k > 1$, define

$$\Delta_k^+ := \langle \phi_{k-2}, \mathcal{A}\phi_k \rangle = \begin{bmatrix} 0 & ka_2^2 & 0 & 0 \\ 0 & 0 & 0 & 0 \\ 0 & 0 & 0 & -ka_2^2 \\ 0 & 0 & 0 & 0 \end{bmatrix}. \tag{1.133}$$

and for $k \geq 1$

$$\Delta_k^- := \langle \phi_{k+2}, \mathcal{A}\phi_k \rangle = \begin{bmatrix} 0 & ka_2^2 & 0 & 0 \\ 0 & 0 & 0 & 0 \\ 0 & 0 & 0 & -ka_2^2 \\ 0 & 0 & 0 & 0 \end{bmatrix}. \tag{1.134}$$

Finally, we write the exogenous input and output matrices for the nonlinear feedback,

$$B = \begin{bmatrix} 0 & 0 \\ 1 & 0 \\ 0 & 0 \\ 0 & 1 \end{bmatrix}, \quad C = \begin{bmatrix} 0 & 0 & 1 & 0 \\ 1 & 0 & 0 & 0 \end{bmatrix} \tag{1.135}$$

and

$$g_k := \begin{bmatrix} g_k^c \\ g_k^s \end{bmatrix} = \int_0^{2\pi} \frac{1}{\sqrt{\pi}} \begin{bmatrix} \cos(k\theta) \\ \sin(k\theta) \end{bmatrix} g(Cx(\theta))\, d\theta. \tag{1.136}$$

Assumptions and Notations

The mistuned thermo-acoustic model described above serves as a specific example motivating the study of, possibly infinite-dimensional, systems with the following structure.

$$\begin{aligned} \dot{x}_1 &= A_1 x_1 + \Delta_2^+ x_2 + Bg(y) && (1.137) \\ \dot{x}_k &= \Delta_{k-1}^- x_{k-1} + A_k x_k + \Delta_{k+1}^+ x_{k+1} + Bg(y), \\ &\quad k = 2, \ldots, \infty \\ y &= Cx \\ x &:= \begin{bmatrix} x_1^T & x_2^T & \ldots \end{bmatrix}^T. && (1.138) \end{aligned}$$

where

$$A_k = A + kA^{(1)} + k^2 A^{(2)} \tag{1.139}$$

$$\Delta_k^+ = \Delta^{(0,+)} + k\Delta^{(1,+)} + k^2\Delta^{(2,+)} \tag{1.140}$$

$$\Delta_k^- = \Delta^{(0,-)} + k\Delta^{(1,-)} + k^2\Delta^{(2,-)} \tag{1.141}$$

Referring to (1.132), for the thermo-acoustic model we have

$$A := \begin{bmatrix} 0 & 0 & 0 & 0 \\ 0 & 0 & K & 0 \\ 0 & 0 & 0 & 0 \\ K & 0 & 0 & 0 \end{bmatrix} \tag{1.142}$$

$$A^{(1)} := \begin{bmatrix} 0 & a_0^2 & 0 & 0 \\ -1 & 0 & 0 & 0 \\ 0 & 0 & 0 & -a_0^2 \\ 0 & 0 & 1 & 0 \end{bmatrix} \tag{1.143}$$

$$A^{(2)} := \begin{bmatrix} -\nu & 0 & 0 & 0 \\ 0 & -\xi & 0 & 0 \\ 0 & 0 & -\nu & 0 \\ 0 & 0 & 0 & -\xi \end{bmatrix}. \tag{1.144}$$

Similarly, referring to (1.133,1.134), for the thermo-acoustic model we have $\Delta^{(0,+)} = \Delta^{(0,-)} = 0, \Delta^{(2,+)} = \Delta^{(2,-)} = 0$, and

$$\Delta^{(1,+)} = \Delta^{(1,-)} = \begin{bmatrix} 0 & a_2^2 & 0 & 0 \\ 0 & 0 & 0 & 0 \\ 0 & 0 & 0 & -a_2^2 \\ 0 & 0 & 0 & 0 \end{bmatrix}. \tag{1.145}$$

The Δ blocks represent coupling between modes with different indices. As shown in (1.137) the $[\cdot]^+$ superscript indicates the influence of mode $k+1$ on mode k and the $[\cdot]^-$ superscript indicates the influence of mode $k-1$ on mode k.

The linear part of the system has a banded infinite-dimensional matrix representation

$$A := \begin{bmatrix} A_1 & \Delta_2^+ & 0 & & 0 \\ \Delta_1^- & A_2 & \Delta_3^+ & \ddots & \\ 0 & \Delta_2^- & A_3 & \Delta_4^+ & 0 \\ & \ddots & \ddots & \ddots & \ddots \\ 0 & & 0 & \ddots & \ddots \end{bmatrix}, \tag{1.146}$$

where all of $A_k, \Delta_k^+, \Delta_k^-$ are the same size. In section 1.3.1 this restriction is partially removed by allowing a larger size A_1 and accordingly zero-padding the matrices Δ_2^+ and Δ_1^-.

The infinite-dimensional matrix representation of a linear operator $\mathcal{P} : L^2(\Omega) \times L^2(\Omega) \to L^2(\Omega) \times L^2(\Omega)$ consists of elements $P_{j,k} \in \mathbb{R}^{n \times n}$, for $j, k = 1, 2, \ldots$, that are defined as follows (see e.g. [1]). If $\mathcal{P}$ is characterized by the kernel $\mathcal{P}(\theta', \theta)$, so that

$$(\mathcal{P}x)(\theta') = \int_\Omega \mathcal{P}(\theta', \theta) x(\theta)\, d\theta$$

then

$$P_{j,k} := \int_\Omega \int_\Omega \phi_j^T(\theta')\mathcal{P}(\theta',\theta)\phi_k(\theta)\, d\theta'\, d\theta. \tag{1.147}$$

For $x, y \in L^2(\Omega)$ we have

$$\langle y, \mathcal{P}x\rangle = \sum_j y_j^T \sum_k P_{j,k}x_k. \tag{1.148}$$

Suppose that $P_{k,k} = P_{k,k}^T$ and that $P_{j,k} = 0$ when $j \neq k$. Hence the infinite-dimensional matrix representation of $\mathcal{P}$ is block-diagonal, and we refer to the operator $\mathcal{P}$ simply as *block-diagonal* with block elements P_k. Then for $x, y \in L^2(\Omega)$ we have

$$\langle y, \mathcal{P}x\rangle = \sum_k y_k^T P_k x_k. \tag{1.149}$$

To show absolute stability, we will use a block-diagonal operator $\mathcal{P}$, characterized by the finite-dimensional matrices P_k, in a Lyapunov function. It is easy to check that if there exists a constant $\sigma > 0$ such that for all $k = 1, 2, \ldots$ the positive definite matrices $P_k > \sigma I$ then $\mathcal{P}$ is coercive (see [31]). This fact will be applied in the forthcoming sections.

We first consider only the linear system

$$\frac{\partial}{\partial t}x = \mathcal{A}x. \tag{1.150}$$

Consider the Lyapunov function $V(x) = \langle x, \mathcal{P}x\rangle$ and assume that $\mathcal{P}$ has a block-diagonal infinite-dimensional matrix representation

$$P := \begin{bmatrix} P_1 & 0 & 0 & \ldots \\ 0 & P_2 & 0 & \ddots \\ 0 & 0 & P_3 & \ddots \\ \vdots & \ddots & \ddots & \ddots \end{bmatrix}, \tag{1.151}$$

where $P_k = \langle \phi_k, \mathcal{P}\phi_k\rangle$ is the same size as A_k. Taking the time derivative of $V(x)$ yields

$$\dot{V} = \langle x, \mathcal{P}\mathcal{A}x\rangle + \langle \mathcal{A}x, \mathcal{P}x\rangle \tag{1.152}$$

$$= \frac{1}{2}\sum_{k\geq 1} x_k^T \left[P_k A_k + A_k^T P_k\right] x_k$$

$$+ \sum_{k\geq 2} \begin{bmatrix} x_{k-1} \\ x_k \end{bmatrix}^T M_k \begin{bmatrix} x_{k-1} \\ x_k \end{bmatrix} \tag{1.153}$$

where

$$M_k = \begin{bmatrix} \Psi_{k-1} & G_k^T \\ G_k & \Psi_k \end{bmatrix} \tag{1.154}$$

$$G_k := \Delta_k^{+T} P_{k-1} + P_k \Delta_{k-1}^{-} \tag{1.155}$$

$$\Psi_k := m_k \left(P_k A_k + A_k^T P_k \right) \tag{1.156}$$

and

$$m_k = \begin{cases} \frac{1}{2}, & k = 1 \\ \frac{1}{4}, & k \geq 2 \end{cases} . \tag{1.157}$$

It is clear that, under suitable conditions, if for all $k = 1, 2, \ldots,$

$$P_k A_k + A_k^T P_k < -\varepsilon \tag{1.158}$$

and

$$M_k \leq 0 \tag{1.159}$$

then the linear system (1.150) is asymptotically stable. We will discuss the suitable conditions in more detail in the next section.

Infinite-Dimensional Absolute Stability

Next, we consider the system with nonlinear coupling. We assume that the nonlinear function $g(u)$ satisfies the spatially constant sector condition, with $\mu \geq 0$,

$$\langle g(u), g(u) - \mu u \rangle \leq 0, \ \ \forall u \in \mathbb{R}. \tag{1.160}$$

Note that the case of a spatially varying sector bound is treated in [31].

Consider the Lyapunov function $V(x) = \langle x, \mathcal{P}x \rangle$, where the bounded linear operator $\mathcal{P}$ is coercive and block diagonal and the matrices P_k are as defined above. Due to the coercivity of $\mathcal{P}$, there exists a matrix $P > 0$ such that $P_k \geq P, \forall k$. From (1.149), $\langle x, \mathcal{P}x \rangle = \sum_k x_k^T P_k x_k$. Taking the time derivative of V, where the necessary regularity conditions are outlined in Chapter 6 of [75], results in

$$\dot{V} = \langle x, \mathcal{P}\mathcal{A}x \rangle + \langle \mathcal{A}x, \mathcal{P}x \rangle - 2\langle x, \mathcal{P}\mathcal{B}g(\mathcal{C}x) \rangle \tag{1.161}$$

$$\leq \langle x, \mathcal{P}\mathcal{A}x \rangle + \langle \mathcal{A}x, \mathcal{P}x \rangle$$
$$- 2\langle x, \mathcal{P}\mathcal{B}g(\mathcal{C}x) \rangle + \ 2\langle [\mu \mathcal{C}x - g(\mathcal{C}x)], g(\mathcal{C}x) \rangle \tag{1.162}$$

$$= \sum_{k \geq 2} \begin{bmatrix} x_{k-1} \\ x_k \end{bmatrix}^T M_k \begin{bmatrix} x_{k-1} \\ x_k \end{bmatrix}$$
$$+ \frac{1}{2} \sum_{k \geq 1} x_k^T \left[P_k A_k + A_k^T P_k \right] x_k$$
$$- 2\langle x, \mathcal{P}\mathcal{B}g(\mathcal{C}x) \rangle + 2\langle [\mu \mathcal{C}x - g(\mathcal{C}x)], g(\mathcal{C}x) \rangle$$

$$= \sum_{k \geq 2} \begin{bmatrix} x_{k-1} \\ x_k \end{bmatrix}^T M_k \begin{bmatrix} x_{k-1} \\ x_k \end{bmatrix}$$
$$+ \sum_{k \geq 1} x_k^T \frac{1}{2} \left[P_k A_k + A_k^T P_k \right] x_k$$
$$+ 2x_k^T \left(\mu C^T - P_k B \right) g_k - 2g_k^T g_k. \tag{1.163}$$

The estimate (1.162) is obtained by applying the sector bound (1.160). For notational convenience we define

$$\begin{aligned}\dot{V}_k :=& x_k^T \frac{1}{2}\left[P_k A_k + A_k^T P_k\right] x_k + 2x_k^T \left(\mu C_e^T - P_k B_e\right) g_k \\ & - 2g_k^T g_k,\end{aligned} \tag{1.164}$$

so according to (1.161-1.164),

$$\dot{V} \leq \sum_{k\geq 2} \begin{bmatrix} x_{k-1} \\ x_k \end{bmatrix}^T M_k \begin{bmatrix} x_{k-1} \\ x_k \end{bmatrix} + \sum_k \dot{V}_k. \tag{1.165}$$

It is now clear that if $M_k < -\varepsilon$ and $\dot{V}_k < 0$ for all k then the system (1.127) will be asymptotically stable. The terms M_k appear due to the linear coupling from mistuning and the terms $\dot{V}_k$ appear due to nonlinear coupling. Each term contains a linear stabilizing part that is used to make the each of the respective terms negative definite.

We will analyze the stability of the infinite-dimensional system by estimating $\dot{V}_k$ for all $k = 1, 2, \ldots$. If there exist constants $\varepsilon > 0$ and $\sigma > 0$ such that for each k, there exists a matrix $P_k > \sigma I > 0$ such that

$$\Gamma_k := P_k A_k + A_k^T P_k + \epsilon \tag{1.166}$$

$$L_k := \mu C^T - P_k B \tag{1.167}$$

$$\Gamma_k + L_k L_k^T \leq 0 \tag{1.168}$$

then (1.164) becomes

$$\begin{aligned}\dot{V}_k \leq & -\varepsilon \frac{1}{2} x_k^T P_k x_k - \frac{1}{2} x_k^T L_k L_k^T x_k + 2x_k^T L_k g_k - 2g_k^T g_k \\ \leq & -\varepsilon \frac{1}{2} x_k^T P_k x_k - \frac{1}{2} x_k^T L_k L_k^T x_k + \frac{1}{2} x_k^T L_k L_k^T x_k \\ \leq & -\varepsilon \frac{1}{2} x_k^T P_k x_k.\end{aligned}$$

We can rewrite (1.168) as an LMI [16]

$$P_k > \sigma I, \quad \begin{bmatrix} \Gamma_k & L_k \\ L_k^T & -I \end{bmatrix} \leq 0, \tag{1.169}$$

which we refer to as the strictly positive real LMI.

Lemma 1.3.1 *If for $k = 1$ the LMI (1.169) is feasible and for $k \geq 2$ the LMI (1.159) and (1.169) are feasible, then system (1.127) is asymptotically stable.*

Proof. Feasibility of LMI (1.169) for $k \geq 1$ implies that $\dot{V}_k \leq -\varepsilon \frac{1}{2} x_k^T x_k$. For $k \geq 2$ feasibility of LMI (1.159) implies that $M_k < 0$. Following (1.165),

$$\dot{V} \leq -\frac{1}{2}\varepsilon \langle x, x \rangle. \tag{1.170}$$

■

Finite Set of LMI Conditions

For practical analysis, one would like to avoid checking the feasibility of an infinite number of LMI. Given the structure of the subsystems, it is possible to establish sufficient conditions so that the feasibility of only a finite number, $N < \infty$, of LMI need be checked. The sufficient conditions establish that if the LMI are feasible for $k = N$ (for some fixed N) then they will be feasible for all $k > N$.

First fix some $N > 1$ which serves as a truncation index. We are concerned with indices $k > N$ so we take $k = N + n$ with $n \geq 1$. Now, for any $n \geq 1$, following (1.139-1.141) we have

$$\begin{aligned} A_{N+n} &= A + (N+n)A^{(1)} + (N+n)^2 A^{(2)} \\ &= A + NA^{(1)} + N^2 A^{(2)} + nA^{(1)} + (2nN + n^2)A^{(2)} \\ &= A_N + nA^{(1)} + (2nN + n^2)A^{(2)} \end{aligned} \tag{1.171}$$

Similarly,

$$\Delta^+_{N+n} = \Delta^+_N + n\Delta^{(1,+)} + (2nN + n^2)\Delta^{(2,+)} \tag{1.172}$$

$$\Delta^-_{N+n} = \Delta^-_N + n\Delta^{(1,-)} + (2nN + n^2)\Delta^{(2,-)}. \tag{1.173}$$

Suppose further that $P_{N+n} = P_N := P$. The finite set of feasibility conditions will be given for the coupling LMI (1.154,1.159) and the strictly positive real LMI (1.169).

Coupling LMI (1.154,1.159)

Define

$$G^{(1)} := \Delta^{(1,+)T} P + P\Delta^{(1,-)} \tag{1.174}$$

$$G^{(2)} := \Delta^{(2,+)T} P + P\Delta^{(2,-)} \tag{1.175}$$

$$\Psi^{(1)} := m_N \left(PA^{(1)} + A^{(1)T} P \right) \tag{1.176}$$

$$\Psi^{(2)} := m_N \left(PA^{(2)} + A^{(2)T} P \right), \tag{1.177}$$

and note that $m_{N+n} = m_N = \frac{1}{4}$. Then,

$$\begin{aligned} G_{N+n} &= \Delta_{N+n}^{+T} P + P\Delta_{N+n-1}^{-} \\ &= \Delta_N^{+T} P + P\Delta_{N-1}^{-} \\ &\quad + n\left(\Delta^{(1,+)T} P + P\Delta^{(1,-)}\right) \\ &\quad + (2nN + n^2)\left(\Delta^{(2,+)T} P + P\Delta^{(2,-)}\right) \\ &= G_N + nG^{(1)} + (2nN + n^2)G^{(2)} \end{aligned} \tag{1.178}$$

$$\begin{aligned} \Psi_{N+n} &= m_N\left(PA_{N+n} + A_{N+n}^T P\right) \\ &= m_N\left(PA_N + A_N^T P\right) \\ &\quad + m_N n\left(PA^{(1)} + A^{(1)T} P\right) \\ &\quad + m_N(2nN + n^2)\left(PA^{(2)} + A^{(2)T} P\right) \\ &= \Psi_N + n\Psi^{(1)} + (2nN + n^2)\Psi^{(2)} \end{aligned} \tag{1.179}$$

and

$$\begin{aligned} \Psi_{N+n-1} &= \Psi_{N-1} + n\Psi^{(1)} + (2n(N-1) + n^2)\Psi^{(2)} \\ &= \Psi_{N-1} + n\Psi^{(1)} - 2n\Psi^{(2)} + (2nN + n^2)\Psi^{(2)}. \end{aligned} \tag{1.180}$$

Following (1.154),

$$\begin{aligned} M_{N+n} &= \begin{bmatrix} \Psi_{N+n-1} & G_{N+n}^T \\ G_{N+n} & \Psi_{N+n} \end{bmatrix} \\ &= M_N + n\begin{bmatrix} \Psi^{(1)} - 2\Psi^{(2)} & G^{(1)T} \\ G^{(1)} & \Psi^{(1)} \end{bmatrix} \\ &\quad + (2nN + n^2)\begin{bmatrix} \Psi^{(2)} & G^{(2)T} \\ G^{(2)} & \Psi^{(2)} \end{bmatrix}. \end{aligned} \tag{1.181}$$

It is easy to show the following:

Lemma 1.3.2 *Suppose that*

$$\begin{bmatrix} \Psi^{(2)} & G^{(2)T} \\ G^{(2)} & \Psi^{(2)} \end{bmatrix} \leq 0 \tag{1.182}$$

and for some $n \geq 1$,

$$\frac{1}{2N+n}\begin{bmatrix} \Psi^{(1)} - 2\Psi^{(2)} & G^{(1)T} \\ G^{(1)} & \Psi^{(1)} \end{bmatrix} + \begin{bmatrix} \Psi^{(2)} & G^{(2)T} \\ G^{(2)} & \Psi^{(2)} \end{bmatrix} \leq 0. \tag{1.183}$$

Then $j > n$ implies that

$$\frac{1}{2N+j}\begin{bmatrix} \Psi^{(1)} - 2\Psi^{(2)} & G^{(1)T} \\ G^{(1)} & \Psi^{(1)} \end{bmatrix} + \begin{bmatrix} \Psi^{(2)} & G^{(2)T} \\ G^{(2)} & \Psi^{(2)} \end{bmatrix} \leq 0. \tag{1.184}$$

Corollary 1.3.3 *Suppose that $M_N \leq 0$ and that for $n = 1$ the LMI (1.182,1.183) hold. Then $M_{N+j} \leq 0$ for all $j \geq 1$.*

Strictly Positive Real LMI (1.169)

From (1.166) and (1.171) it follows that

$$\begin{aligned}\Gamma_{N+n} &:= PA_{N+n} + A_{N+n}^T P + \epsilon \\ &= \Gamma_N + n\left(PA^{(1)} + A^{(1)T}P\right) \\ &\quad + (2nN + n^2)\left(PA^{(2)} + A^{(2)T}P\right) \end{aligned} \tag{1.185}$$

As in lemma 1.3.2, it is easy to show the following:

Lemma 1.3.4 *Suppose that*

$$PA^{(2)} + A^{(2)T}P \leq 0 \tag{1.186}$$

and for some $n \geq 1$,

$$\frac{1}{2N+n}\left(PA^{(1)} + A^{(1)T}P\right) + \left(PA^{(2)} + A^{(2)T}P\right) \leq 0. \tag{1.187}$$

Then $j > n$ implies that

$$\frac{1}{2N+j}\left(PA^{(1)} + A^{(1)T}P\right) + \left(PA^{(2)} + A^{(2)T}P\right) \leq 0. \tag{1.188}$$

Corollary 1.3.5 *Suppose that for index $k = N$, $P > \sigma I$ satisfies (1.169) and (1.186,1.187) with $n = 1$. Then P is a feasible solution of the LMI (1.169) for all $k \geq N$.*

Proof. Because $P_{N+n} = P$ is constant over n, the only entry in (1.169) that varies with n is the $(1,1)$ entry. Feasibility of (1.186,1.187) ensures that $\Gamma_{N+j} \leq \Gamma_{N+n}$ when $j \geq n$. ∎

Model Truncation

Restricting the Lyapunov function to be block diagonal can be overly conservative. This restriction can be partially reduced by allowing allowing larger block sizes. In this section we consider a larger finite-dimensional model and analyze the feasibility of the LMI. This allows at least the first block to be arbitrarily large, but finite. Extending the analysis to apply to larger subsequent blocks is straightforward and not explicitly discussed here.

For some $N > 1$ define truncated finite-dimensional model $A_B \in \mathbb{R}^{(N-1)n \times (N-1)n}$,

$$A_B := \begin{bmatrix} A_1 & \Delta_2^+ & 0 & & 0 \\ \Delta_1^- & A_2 & \Delta_3^+ & \ddots & \\ 0 & \Delta_2^- & A_3 & \Delta_4^+ & 0 \\ & \ddots & \ddots & \ddots & \Delta_{N-1}^+ \\ 0 & & 0 & \Delta_{N-2}^- & A_{N-1} \end{bmatrix}, \tag{1.189}$$

$$B_B = diag\{B, \ldots, B\}, \;\; C_B = diag\{C, \ldots, C\} \tag{1.190}$$

and

$$x_B := \left[\begin{array}{ccc} x_1^T & \ldots & x_{N-1}^T \end{array} \right]^T \tag{1.191}$$

$$g_B := \left[\begin{array}{ccc} g_1^T & \ldots & g_{N-1}^T \end{array} \right]^T. \tag{1.192}$$

In each of (1.189,1.190) the 0 blocks are assumed to be appropriately sized matrices. Consider a block-diagonal Lyapunov function

$$V(x) = \langle x, \mathcal{P}x \rangle = x_B^T P_B x_B + \sum_{k \geq N} x_k^T P_k x_k \tag{1.193}$$

where $P_B \in \mathbb{R}^{(N-1)n \times (N-1)n}$ and $P_k \in \mathbb{R}^{n \times n}$ for $k \geq N$. Following (1.154-1.156) define

$$M_B = \left[\begin{array}{cc} \Psi_B & G_B^T \\ G_B & \Psi_N \end{array} \right] \tag{1.194}$$

where

$$G_B := \Delta_B^{+T} P_B + P_N \Delta_B^- \tag{1.195}$$

$$\Psi_B := \frac{1}{2} \left(P_B A_B + A_B^T P_B \right) \tag{1.196}$$

and

$$\Delta_B^{+T} := \left[\begin{array}{cccc} 0 & \ldots & 0 & \Delta_N^{+T} \end{array} \right] \in \mathbb{R}^{n \times (N-1)n} \tag{1.197}$$

$$\Delta_B^- := \left[\begin{array}{cccc} 0 & \ldots & 0 & \Delta_{N-1}^- \end{array} \right] \in \mathbb{R}^{n \times (N-1)n} \tag{1.198}$$

and $\Psi_N = \frac{1}{4} \left(P_N A_N + A_N^T P_N \right)$ by (1.156).

Taking the time derivative of $V(x)$ and applying the sector bound (1.160) results in

$$\dot{V} \leq x_B^T \frac{1}{2} \left[P_B A_B + A_B^T P_B \right] x_B \tag{1.199}$$

$$+ 2x_k^B \left(\mu C_B^T - P_B B_B \right) g_B - 2 g_B^T g_B \tag{1.200}$$

$$+ \left[\begin{array}{c} x_B \\ x_N \end{array} \right]^T M_B \left[\begin{array}{c} x_B \\ x_N \end{array} \right] \tag{1.201}$$

$$+ \sum_{k \geq N+1} \left[\begin{array}{c} x_{k-1} \\ x_k \end{array} \right]^T M_k \left[\begin{array}{c} x_{k-1} \\ x_k \end{array} \right] \tag{1.202}$$

$$+ \sum_{k \geq N} x_k^T \frac{1}{2} \left[P_k A_k + A_k^T P_k \right] x_k \tag{1.203}$$

$$+ 2x_k^T \left(\mu C^T - P_k B \right) g_k - 2 g_k^T g_k. \tag{1.204}$$

Define

$$\Gamma_B := P_B A_B + A_B^T P_B + \epsilon \tag{1.205}$$

$$L_B := \mu C_B^T - P_B B_B \tag{1.206}$$

and consider the LMI analogous to (1.169)

$$P_B > \sigma I, \quad \begin{bmatrix} \Gamma_B & L_B \\ L_B^T & -I \end{bmatrix} \leq 0. \tag{1.207}$$

Theorem 1.3.6 *Given some positive truncation index $N > 1$. Suppose the following conditions hold:*

1. *P_B satisfies LMI (1.207)*
2. *P_N satisfies LMI $M_B \leq 0$*
3. *P_N satisfies LMI (1.182,1.183) with $n = 1$*
4. *P_N satisfies LMI (1.186,1.187) with $n = 1$*

Then the system (1.137) is absolutely stable with respect to feedback nonlinearities satisfying (1.160).

Proof. Take the Lyapunov function

$$V(x) = \langle x, \mathcal{P}x \rangle = x_B^T P_B x_B + \sum_{k \geq N} x_k^T P_N x_k. \tag{1.208}$$

The stated conditions ensure that the terms in (1.199-1.204) are negative:

1. implies that (1.199,1.200) $\leq -\epsilon x_B^T x_B$.
2. implies that (1.201) ≤ 0.
3. implies that (1.202) ≤ 0.
4. implies that (1.203,1.204) $\leq -\epsilon \sum_{k \geq N} x_k^T x_k$.

Together these imply that $\dot{V} \leq -\epsilon \|x\|$. Furthermore, since the infinite-dimensional matrix representation of $\mathcal{P}$ is block diagonal consisting of the two finite-dimensional blocks P_B and P_N, the operator $\mathcal{P}$ is coercive and bounded. ∎

Numerical Results

In this section we present numerical results concerning the solutions of the LMI given in the previous sections. We consider the PDE system (1.123,1.124) with wave-speed mistuning and a feedback nonlinearity satisfying a sector bound. As discussed in [7],[26] it is known that wave-speed mistuning acts to stabilize thermo-acoustic systems with skew-symmetric heat-release coupling. However, in these cases the results were established only for finite-dimensional models. The model parameters were chosen such that the system without mistuning is unstable and develops a limit-cycle oscillation. A wave-speed mistuning parameter along with truncation index N was chosen such that the conditions of theorem 1.3.6 were satisfied. The response of the acoustic pressure $p(\theta, t)$ is shown in figure 1.18. Initially the system has no mistuning and develops a limit-cycle due to the skew-symmetric feedback. At $t = 25$ the wave-speed mistuning is applied and the system stabilizes to the uniform steady solution.

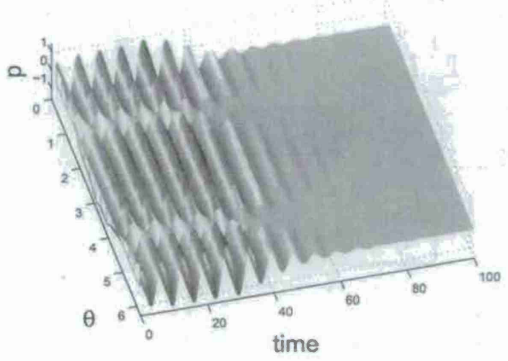

Figure 1.18: wave-speed mistuning initially turned off. Turned on at time= 25.

1.3.2 Coupling of Stable Subsystems

In many applications, feedback interconnections between stable dynamical subsystems can lead to instability or high sensitivity. Examples of such instabilities include beam vibration [6, 12], flutter instabilities [?], and large platoons of vehicles [?, ?, ?, 39, 8]. Often, the dynamic models of these systems are characterized by a large number of similar subsystems through neighboring coupling, and the coupling of the subsystems may have aperiodic or random patterns [70, 60]. As a result, stability analysis of such dynamical systems becomes a challenge.

Under this contract, we considered coupling of arbitrarily many stable subsystems connected in a chain form (see Figure 1.19), and we studied how stability and robustness evolve for varying coupling gains between neighboring subsystems. In particular, we focused on linear stable subsystems that have a property of "*negative imaginary frequency response*" [44], which basically means that the subsystem's phase shift angle is within the range of $[-\pi, 0]$ and closely relates to the property of *counterclockwise input-output dynamics* studied in [2]. We call them *stable negative imaginary* (SNI) systems. It has

been shown in [44] that stability for a positive feedback interconnection of two SNI subsystems can be checked by their DC gain (i.e. the loop gain at zero frequency); see Figure 1.20.

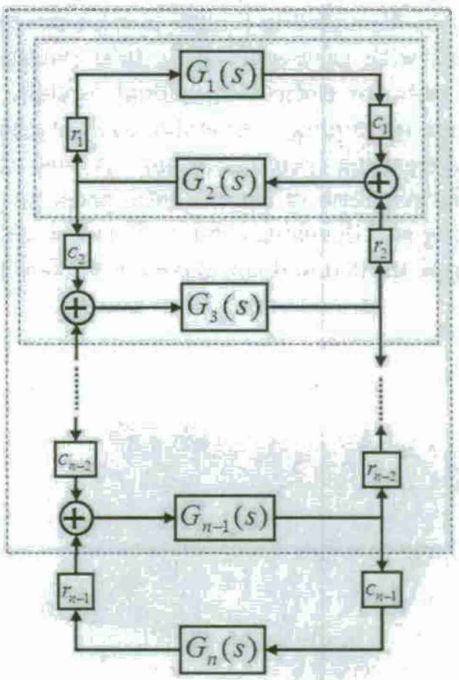

Figure 1.19: String of n coupled SNI

The string of n SNI subsystems is simply the coupling of n SNI subsystems via neighboring positive feedback interconnection. Following [44, 2], we characterized the stability of the string through convergence of a continued fraction that denotes DC gain of sequentially coupled subsystems. The derived results avoid explicit computation of eigenvalues or construction of Lyapunov functions, and they are readily applicable to analyzing stability and robustness of dynamical systems with different coupling patterns.

Similar analysis was also extended to a ring form (See Figure 1.21).

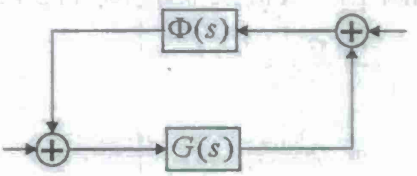

Figure 1.20: Positive feedback interconnection of two subsystems $G(s)$ and $\Phi(s)$.

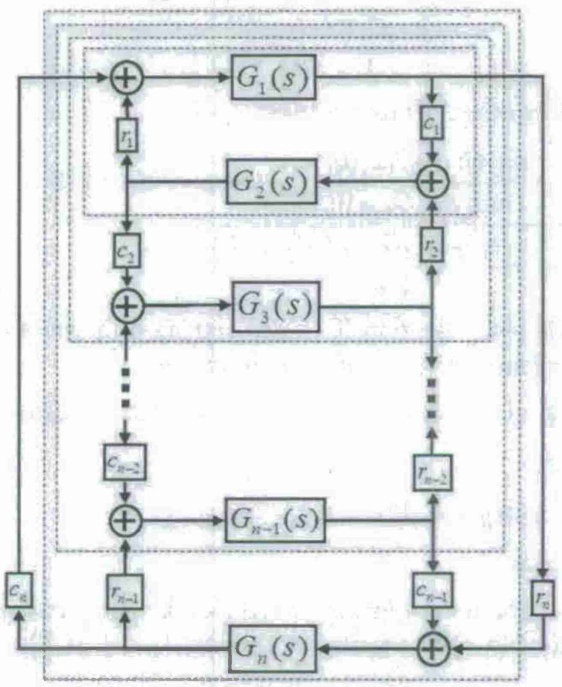

Figure 1.21: Ring of n coupled SNI

The String Form of Coupling

Denote by $\Phi_i(s)$ the transfer function of the first $(i+1)$ coupled subsystems (see the transfer functions contoured by dashed squares in Figure 1.19). Inductively, we obtain that,

$$\begin{aligned}\Phi_1(s) =& \frac{G_2(s)}{1 - c_1 r_1 G_1(s) G_2(s)},\\ \Phi_i(s) =& \frac{G_{i+1}(s)}{1 - c_i r_i \Phi_{i-1}(s) G_{i+1}(s)} \quad \forall i = 2, 3, \cdots, n-2.\end{aligned}$$

Thus the string of n coupled stable subsystems is exactly the positive feedback interconnection of $\Phi_{n-2}(s)$ and $c_{n-1} r_{n-1} G_n(s)$. Also, denote the DC loop gains of coupled subsystems as follows:

$$\lambda_1 = c_1 r_1 G_1(0) G_2(0)$$

and, for each $i = 2, 3, \cdots, n-1$,

$$\begin{aligned}\lambda_i :=& c_i r_i \Phi_{i-1}(0) G_{i+1}(0)\\ =& \frac{c_i r_i G_i(0) G_{i+1}(0)}{1 - c_{i-1} r_{i-1} \Phi_{i-2}(0) G_i(0)}\\ =& \frac{c_i r_i G_i(0) G_{i+1}(0)}{1 - \lambda_{i-1}}.\end{aligned}$$

Clearly, each λ_i is a continued fraction. Thus we have

$$\lambda_i = \cfrac{c_i r_i G_i(0) G_{i+1}(0)}{1 + \cfrac{- c_{i-1} r_{i-1} G_{i-1}(0) G_i(0)}{1 + \cfrac{- c_{i-2} r_{i-2} G_{i-2}(0) G_{i-1}(0)}{1 + \cdots}}} \quad \forall i = 2, 3, \cdots, n-1. \tag{1.209}$$

The following result extends [44, Theorem 5] to the setting of a series of coupled SNI by relating stability of the string to convergence of the continued fractions.

Theorem 1.3.7 *For the string of n coupled SNI, if G_1 is a SNI subsystem in a strict sense,*

- *$G_i(\infty) = 0$ for all $i = 1, 2, \cdots, n$,*
- *λ_i in (1.209) is less than unity for all $i = 1, 2, \cdots, n-1$,*

then the string is internally stable.

The next result presents a sufficient condition in term of the subsystems' DC gains and their local coupling gains for guaranteeing that each continued fraction $\lambda_i < 1$ in Theorem 1.3.7.

Theorem 1.3.8 *The string of n coupled SNI is internally stable if G_1 is a SNI subsystem in a strict sense, $G_i(\infty) = 0$ for all $i = 1, 2, \cdots, n$, and*

$$\begin{cases} c_1 r_1 G_1(0) G_2(0) < \frac{1}{2}, \\ c_i r_i G_i(0) G_{i+1}(0) \le \frac{1}{4} \quad \forall i = 2, \cdots, n-2, \\ c_{n-1} r_{n-1} G_{n-1}(0) G_n(0) \le \frac{1}{2} \text{ (if } n > 2). \end{cases} \tag{1.210}$$

The Ring Form of Coupling

It turns out that Theorem 1.3.8 can be extended to a ring form (See Figure 1.21).

Theorem 1.3.9 *The ring of n coupled SNI subsystems is internally stable if G_1 is a SNI subsystem in a strict sense, $\prod_{i=1}^{n} c_i = \prod_{i=1}^{n} r_i$, and $G_i(0) \geq 0$ and $G_i(\infty) = 0$ for all $i = 1, 2, \cdots, n$, and*

$$\begin{cases} c_i r_i G_i(0) G_{i+1}(0) \leq \frac{1}{4} & \forall i = 1, \cdots, n-1, \\ c_n r_n G_1(0) G_n(0) < \frac{1}{4}, \end{cases} \tag{1.211}$$

Robust Stability for the String

The quantity λ_{n-1} as defined in (1.209) can be regarded as "robustness" of stability for the string of n coupled stable subsystems. It is interesting to see how varying coupling gains make λ_{n-1} approach its limits (typically less than unity) as the dimension n increases to infinity. For $\lambda_{n-1} < 1$, the string remains stable with respect to small variations of neighbor-coupling gains and certain unmodeled dynamics that also belongs to the class of SNI.

In Theorem 1.3.8, consider the case of $c_i r_i G_i(0) G_{i+1}(0) = \frac{1-\mu^2}{4}$ for all $i = 1, 2, \cdots, n-1$, where $\mu \in [0, 1)$ is called a mistuning parameter. Solving the equation $\lambda = \frac{1-\mu^2}{4} \cdot \frac{1}{1-\lambda}$ gives $\lambda = \frac{1 \pm \mu}{2}$. We verify that if $0 \leq \lambda_i < \frac{1-\mu}{2}$ then $\lambda_{i+1} > \lambda_i$ and $\lim_{i \to \infty} \lambda_i = \dfrac{1-\mu}{2}$. Also, we verify that if $\lambda_i = \frac{1-\mu}{2} - \varepsilon$, where $0 \leq \varepsilon < \frac{1-\mu}{2}$, then

$$\lambda_{i+1} = \frac{1-\mu}{2} - \frac{(1-\mu)\varepsilon}{1+\mu+2\varepsilon} \leq \frac{1-\mu}{2} - \frac{\sigma\varepsilon}{1+2\varepsilon},$$

where $\sigma = \frac{1-\mu}{1+\mu}$ and the equality holds for $\mu = 0$. Consequently, we establish by induction that, for each $i = 1, 2, \cdots, n-1$,

- if $\mu = 0$ then

$$\lambda_i = \frac{1}{2} - \frac{\varepsilon}{1 + 2\varepsilon(i-1)}$$

  and hence λ_i approaches its limit $\frac{1}{2}$ in the order of $\mathcal{O}(\frac{1}{i})$ as i increases, and

- if $0 < \mu < 1$ then

$$\lambda_i \leq \frac{1-\mu}{2} - \frac{\sigma^i \varepsilon}{1 + 2\varepsilon \sum_{m=1}^{i} \sigma^{m-1}} \leq \frac{1-\mu}{2} - \frac{\sigma^i \varepsilon}{1 + \frac{2\varepsilon}{1-\sigma}}$$

  and hence λ_i approaches its limit $\frac{1-\mu}{2}$ in the order of at most $\mathcal{O}(\sigma^i)$ as i increases.

For the general case of $c_i r_i G_i(0) G_{i+1}(0) \leq \frac{1-\mu^2}{4}$ $(i = 1, 2, \cdots, n-1)$, the above convergence statements still hold, which is used for estimating the values of the continued fractions and their approximants, allows the parameters $|\kappa_i| \leq 1$.

Application: Decentralized Control of Vehicle Platoons

As an application, we considered a platoon of n vehicles modeled as follows

$$\ddot{y}_i = u_i \quad \forall i = 1, 2, \cdots, n, \tag{1.212}$$

where y_i and u_i are the position and control input of the i^{th} vehicle, respectively. The control objective is to maintain a desired distance $L > 0$ between any two neighboring vehicles and ensure a desired velocity $V > 0$ for each vehicle, provided that each vehicle has the spacing and velocity information relative to its front and back ones. Denote $\delta_i(t) = y_i(t) - y_{i-1}(t) + L$.

Two control strategies are provided as follows. The first one is designed with control inputs:

$$\begin{aligned}
u_1(t) &= -\xi_1(\dot{y}_1(t) - V) - F_1(y_1(t) - Vt) + B_1\delta_2(t), \\
u_i(t) &= -\xi_i(\dot{y}_i(t) - V) - F_i\delta_i(t) + B_i\delta_{i+1}(t) \qquad \forall i = 2, 3, \cdots, n-1, \\
u_n(t) &= -\xi_n(\dot{y}_n(t) - V) - F_n\delta_n(t),
\end{aligned}$$

where each ξ_i is a damping parameter and each F_i (respectively, B_i) is a control gain due to the difference between the positions of the i^{th} vehicle and its front (respectively, back) one. This control strategy requires all vehicles to have a priori knowledge of the desired velocity V.

Using the previous stability results, we established that the system (1.212) achieves asymptotic tracking with positive real constants ξ_i, F_i, and B_i $(i = 1, 2, \cdots, n)$ is internally stable.

As the second control strategy, we apply the following control inputs:

$$\begin{aligned}
u_1(t) &= -F_1(y_1(t) - Vt + L) - \hat{\kappa}F_1(\dot{y}_1(t) - V) + B_1\delta_2(t) + \kappa B_1\dot{\delta}_2(t), \\
u_i(t) &= -F_i\delta_i(t) - \kappa F_i\dot{\delta}_i(t) + B_i\delta_{i+1}(t) + \kappa B_i\dot{\delta}_{i+1}(t) \qquad \forall i = 2, 3, \cdots, n-1, \\
u_n(t) &= -F_n\delta_n(t) - \kappa F_n\dot{\delta}_n(t)
\end{aligned}$$

where $\hat{\kappa} > \kappa > 0$ are constants and each F_i (respectively, B_i) is a control gain due to the spacing and velocity differences between the i^{th} vehicle and its front (respectively, back) one. This control strategy requires only the leading vehicle has the information of the desired velocity V for the platoon.

Again, using the previous stability results, we established that the system (1.212) achieves asymptotic tracking with positive real constants $\hat{\kappa} > \kappa$, F_i and B_i $(i = 1, 2, \cdots, n)$.

These stability results for large vehicle platoon can serve as a foundation for designing various coupling patterns and/or gains so as to enhance robust stability or improve system performance.

Chapter 2

Transitions of past AFOSR-sponsored research at UTRC

2.1 Nonlinear Dynamic Texture Modeling

The concepts developed for nonlinear dynamic texture modeling were applied in an internally funded project to calibrate dynamic models from synchronized high-speed video and acoustic press. POC Tory Brogan, Pratt & Whitney, 860 557 0547.

Chapter 3

Personnel Supported

UTRC personnel: Gregory Hagen, Chaohong Cai, George Mathew, Andrzej Banaszuk, Alberto Speranzon .

Chapter 4

Publications

4.1 Journal papers

[j1] C. Cai and G. Hagen, Stability analysis for a string of coupled stable subsystems with negative imaginary frequency response. To appear in: IEEE Transactions on Automatic Control, 2010.

[j2] G. Hagen, Stochastic Averaging for Identification of Feedback Nonlinearities in Thermo-Acoustic Systems. Provisionally accepted: ASME Journal on Dynamic Systems, Measurement, and Control, 2010.

4.2 Journal papers in preparation

[p1] U. Vaidya and G. Hagen, Model Reduction of Nonlinear Systems, Tangent Space Approach. In preparation

[p2] C. Cai and G. Hagen, Stability analysis for a Ring of Coupled Negative Imaginary Systems. In preparation

[p3] G. Hagen and A. Speranzon, Locally Affine Switched Dynamic Texture Models. In preparation

[p4] G. Hagen, On Dynamic Mode Decomposition and Dynamic Texture Models. In preparation

[p5] G. Hagen and A. Speranzon, Tangent Space Approximation Approach to Compressed Sensing and Dictionary Optimization. In preparation

4.3 Conference papers

[c1] J. Cohen, G. Hagen, A. Banaszuk, S. Becz, P. Mehta, "Attenuation Of Gas Turbine Combustor Pressure Oscillations Using Symmetry Breaking", AIAA Aerospace Sciences Meeting, 2011, Orlando, FL.

[c2] G. Hagen, Absolute Stability of a Dissipative Wave Equation with Waves-Speed Mistuning. Proceedings of the American Control Conference, Baltimore, MD. 2010.

[c3] U. Vaidya, G. Hagen, Model reduction of nonlinear systems: Tangent space approach. Proceedings of the American Control Conference, Baltimore, MD. 2010.

[c4] C. Cai, G. Hagen, Coupling of Stable Systems with Counterclockwise Input-output Dynamics. Proceedings of the American Control Conference, Baltimore, MD. 2010.

[c5] C. Cai, G. Hagen, Stability Results for String of Stable Subsystems with Applications to Decentralized Control of Large Vehicle Platoons, Proceedings of the 48th IEEE Conference on Decision and Control/ 28th Chinese Control Conference, Shanghai, China, 2009

[c6] M. Arienti, M. C. Soteriou, G. Hagen, M. L. Corn, Analysis of Liquid Jet Atomization Dynamics Using Proper Orthogonal Decomposition, 47th AIAA Aerospace Sciences Meeting Including The New Horizons Forum and Aerospace Exposition, 5 - 8,Orlando, Florida, January 2009.

[c7] M. Arienti , M. Corn, G. S. Hagen, R. K. Madabhushi and M. C. Soteriou, Proper Orthogonal Decomposition Applied to Liquid Jet Dynamics, ILASS Americas, 21st Annual Conference on Liquid Atomization and Spray Systems, Orlando, Florida, May 2008.

[c8] S. Meyn, G. Hagen, G. Mathew, A. Banaszuk, On Complex Spectra and Metastability of Markov Models, Proceedings of the 47th IEEE Conference on Decision and Control, Cancun, Mexico, 2008

[c9] G. Hagen, U. Vaidya, An Approach for Nonlinear Model Extraction from Time-Series Data. Proceedings of the American Control Conference, Seattle, WA. 2008.

Bibliography

[1] N. I. Akhiezer and I. M. Glazman. *Theory of Linear Operators in Hilbert Space vol. 1 and 2.* Dover, 1993.

[2] D. Angeli. Systems with counter-clockwise input-output dynamics. *IEEE Transactions on Automatic Control*, 51:1130–1143, 2006.

[3] K.S. Arun and S.Y. Kunch. Balanced approximation of stochastic systems. *SIAM Journal on Matrix Analysis and Applications*, 11(1):42–68, 1990.

[4] I. Awasthi and A Elgammal. Learning nonlinear manifolds of dynamic textures. pages 395–405. Springer-Verlag, 2007.

[5] S. Balaji and S. P. Meyn. Multiplicative ergodicity and large deviations for an irreducible Markov chain. *Stoch. Proc. Applns.*, 90(1):123–144, 2000.

[6] M. J. Balas. Active control of flexible systems. *Journal of Optimization Theory and Applications*, 25(3):415–436, 1978.

[7] A. Banaszuk, P. Mehta, and G. Hagen. The role of control in design: From fixing problems to the design of dynamics. *Control Engineering Practice*, 15(10):1195–1318, 2007.

[8] P. Barooah, P. G. Mehta, and J. P. Hespanha. Mistuning-based decentralized control of vehicular platoons for improved closed loop stability. *IEEE Transactions on Automatic Control, to appear, (http://mechse.illinois.edu/sites/index.php?id=442|Publications)*, 2009.

[9] C. Beck, J. Doyle, and K. Glover. Model reduction of multidimensional and uncertain systems. *IEEE Transaction on Automatic Control*, 41:1466–1477, 1996.

[10] O. O. Bendiksen. Localization phenomena in structural dynamics. *Chaos, Solitons, and Fractals*, 11:1621–1660, 2000.

[11] G. Berkooz, P. Holmes, and J. L. Lumley. The proper orthogonal decomposition in the analysis of trubulent flows. *Annu. Rev. Fluid Mech.*, 25:539–575, 1993.

[12] J. Bontsema and R. F. Curtain. A note on spillover and robustness for flexible systems. *IEEE Transactions on Automatic Control*, 33(6):567–569, 1988.

[13] A. Bovier, M. Eckhoff, V. Gayrard, and M. Klein. Metastability in stochastic dynamics of disordered mean-field models. *Probab. Theory Related Fields*, 119(1):99–161, 2001.

[14] Anton Bovier, Michael Eckhoff, Véronique Gayrard, and Markus Klein. Metastability in reversible diffusion processes. I. Sharp asymptotics for capacities and exit times. *J. Eur. Math. Soc. (JEMS)*, 6(4):399–424, 2004.

[15] Anton Bovier, Véronique Gayrard, and Markus Klein. Metastability in reversible diffusion processes. II. Precise asymptotics for small eigenvalues. *J. Eur. Math. Soc. (JEMS)*, 7(1):69–99, 2005.

[16] S. Boyd, L. El Ghaoui, E. Feron, and V. Balakrishnan. *Linear Matrix Inequalities in System and Control Theory*. SIAM Studies in Applied Mathematics, 1994.

[17] J. Cohen, G. Hagen, A. Banaszuk, S. Becz, and P. Mehta. Attenuation of combustor pressure oscillations using symmetry breaking. *Submitted to 49th AIAA Aerospace Sciences Meeting*, 2011.

[18] F. E. Culick. Nonlinear behavior of acoustic waves in combustion chambers, parts I and II. *Acta Astronautica*, 3:715–757, 1976.

[19] M. Dellnitz and O. Junge. On the approximation of complicated dynamical behavior. *SIAM Journal on Numerical Analysis*, 36:491–515, 1999.

[20] M. Dellnitz and O. Junge. *Set oriented numerical methods for dynamical systems*, pages 221–264. World Scientific, 2000.

[21] P. Deuflhard, W. Huisinga, A. Fischer, and Ch. Schütte. Identification of almost invariant aggregates in reversible nearly uncoupled Markov chains. *Linear Algebra Appl.*, 315(1-3):39–59, 2000.

[22] Persi Diaconis and Daniel Stroock. Geometric bounds for eigenvalues of Markov chains. *Ann. Appl. Probab.*, 1:36–61, 1991.

[23] G. Doretto, A. Chiuso, Y.N. Wu, and S. Soatto. Dynamic textures. *International Journal of Computer Vision*, 51(2):91–109, 2003.

[24] G. Dullerud and R. D'Andrea. Distributed control of inhomogeneous systems with boundary conditions. *Proceedings of the 38th IEEE Control Conference on Decision and Control*, pages 186–190, 1999.

[25] G. Dullerud and S. Lall. A new approach for analysis and synthesis of time-varying systems. *IEEE Transaction on Automatic Control*, 44:1486–1497, 1999.

[26] B. Eisenhower, G. Hagen, A. Banaszuk, and I. Mezić. Passive control of limit cycle oscillations in a thermoacoustic system using asymmetry. *ASME Journal of Applied Mechanics*, 75(1):1–9, 2008.

[27] P. A. Ferrari, H. Kesten, and S. Martínez. *R*-positivity, quasi-stationary distributions and ratio limit theorems for a class of probabilistic automata. *Ann. Appl. Probab.*, 6:577–616, 1996.

[28] G. Ferrari-Trecate, M. Muselli, D. Liberati, and M. Morari. A clustering technique for the identification of piecewise affine systems. *Automatica*, 39:205–217, 2003.

[29] J. A. Fill. Eigenvalue bounds on convergence to stationarity for nonreversible Markov chains, with an application to the exclusion process. *Ann. Appl. Probab.*, 1(1):62–87, 1991.

[30] D. Givon, R. Kupferman, and A. Stuart. Extracting macroscopic dynamics: model problems and algorithms. *Nonlinearity*, 17:55–127, 2004.

[31] G. Hagen. Absolute stability of a heterogeneous semilinear dissipative parabolic pde. *Proceedings of the 43rd IEEE Conference on Decision and Control*, 2004.

[32] G. Hagen. Absolute stability via boundary control of a semilinear parabolic pde. *IEEE Transactions on Automatic Control*, 2006.

[33] G. Hagen and A. Banaszuk. Uncertainty propagation in a reduced order thermo-acoustic model. *Proceedings of the 43rd IEEE Conference on Decision and Control*, 2004.

[34] D. Hinrichsen and A.J. Pritchard. An improved error estimate for reduced-order models of discrete-time systems. *IEEE Transaction on Automatic Control*, 35:317–320, 1990.

[35] P. Holmes, J. L. Lumley, and G. Berkooz. *Turbulence, Coherent Structures, Dynamical Systems and Symmetry*. Cambridge University Press, Cambridge, 1998.

[36] R. A. Horn and C. R. Johnson. *Matrix Analysis*. Cambridge University Press, Cambridge, 1996.

[37] W. Huisinga. *Metastability of Markovian Systems: A transfer Operator approach to molecular dynamics*. PhD thesis, Free University Berlin, 2001.

[38] W. Huisinga, S. Meyn, and C. Schutte. Phase transitions and metastability in Markovian and molecular systems. *The Annals of Applied Probability*, 14(1):419–458, 2004.

[39] M. R. Jovanovic and B. Bamieh. On the ill-posedness of certain vehicular platoon control problems. *IEEE Transactions on Automatic Control*, 50:1307–1321, 2005.

[40] M. R. Jovanovic, B. Bamieh, and M. Grebeck. Parametric resonance in spatially distributed systems. *Proceedings of the 2003 American Control Conference, Denver, CO.*, pages 119–124, 2003.

[41] I. Kontoyiannis and S. P. Meyn. Spectral theory and limit theorems for geometrically ergodic Markov processes. *Ann. Appl. Probab.*, 13:304–362, 2003. Presented at the INFORMS Applied Probability Conference, NYC, July, 2001.

[42] S. Lall and C. Beck. Error-bounds for balanced model reduction of time-varying systems. *IEEE Transaction on Automatic Control*, 48(6):946–956, 2001.

[43] S. Lall, J. E. Marsden, and S. Glavaski. A subspace approach to balanced truncation for model reduction of nonlinear control systems. *International Journal on Robust and Nonlinear Control*, 12:519–535, 2002.

[44] A. Lanzon and I. R. Petersen. Stability robustness of a feedback interconnection of systems with negative imaginary frequency response. *IEEE Transactions on Automatic Control*, 53:1042–1046, 2008.

[45] A. Lasota and M. C. Mackey. *Chaos, Fractals, and Noise: Stochastic Aspects of Dynamics.* Springer-Verlag, New York, 1994.

[46] C.-K. Li, R.-C. Li, and Q. Ye. Eigenvalues of an alignment matrix in nonlinear manifold learning. *Communications in Mathematical Sciences*, 5(2):313–329, 2007.

[47] R.-S. Lin, C.-B. Liu, M.-H. Yang, N. Ahuja, and S. Levinson. Learning nonlinear manifolds from time series. pages 245–256. Springer-Verlag, 2006.

[48] C.-B. Liu, R.-S. Lin, N. Ahuja, and M.-H. Yang. Dynamic textures synthesis as nonlinear manifold learning and traversing. *Procedings of the 17th British Machine Vision Conference*, 2006.

[49] L. Ljung. *System Identification Theory for the User.* Prentice Hall, 2nd edition edition, 1999.

[50] P. Mehta, G. Hagen, and A. Banaszuk. Symmetry and symmetry-breaking for a wave equation with feedback. *SIAM Journal on Applied Dynamical Systems*, 6(3), 2007.

[51] P. G. Mehta and U. Vaidya. On stochastic analysis approaches for comparing dynamical systems. In *Proceeding of IEEE Conference on Decision and Control*, pages 8082–8087, Spain, 2005.

[52] I. Mezić. Spectral properties of dynamical systems, model reductions and decompositions. *Nonlinear Dynamics*, 2005.

[53] I. Mezić and A. Banaszuk. Comparison of systems with complex behavior. *Physica D*, 197:101–133, 2004.

[54] B. C. Moore. Principal component analysis in linear systems: controllability, observability, and model reduction. *IEEE Transaction on Automatic Control*, 26:17–32, 1981.

[55] P. M. Morse and K. U. Ingard. *Theoretical Acoustics.* Princeton University Press, 1968.

[56] H. Nakada, K. Takaba, and T. Katayama. Identification of piecewise affine systems based on statistical clustering technique. *Automatica*, 41:905–913, 2005.

[57] E. Nummelin. *General Irreducible Markov Chains and Nonnegative Operators.* Cambridge University Press, Cambridge, 1984.

[58] E. P. Petrov, R. Vitali, and R. T. Haftka. Optimization of mistuned bladed discs using gradient-based response surface approximations. *AIAA-2000-1522*, 2000.

[59] L. Rey-Bellet and L. E. Thomas. Asymptotic behavior of thermal nonequilibrium steady states for a driven chain of anharmonic oscillators. *Comm. Math. Phys.*, 215(1):1–24, 2000.

[60] A. J. Rivas-Guerra and M. P. Mignolet. Local/global effects of mistuning on the forced response of bladed disks. *Journal of Engineering for Gas Turbines and Power*, 125:1–11, 2003.

[61] J. Roll, A. Bemporad, and L. Ljung. Identification of piecewise affine systems via mixed-integer programming. *Automatica*, 40:37–50, 2004.

[62] C. Rowley. Model reduction for fluids, using balanced proper orthogonal decomposition. *International Journal on Bifurcation and Chaos*, 15(3):997–1013, 2005.

[63] C. Rowley, I. Mezic, S. Bagheri, P. Schlatter, and D. S. Henningson. Spectral analysis of nonlinear flows. *Journal of Fluid Mechanics*, 2009.

[64] T. Runolfsson and Y. Ma. Model reduction of nonreversible Markov chains. *Proceedings of the 46th IEEE Conference on Decision and Control*, 2007.

[65] J. M. A Scherpen. Balancing for nonlinear systems. *Systems and control letters*, 21(2):143–153, 1993.

[66] P. J. Schmid. Dynamic mode decomposition of experimental data. *8th international symposium on particle image velocimetry - PIV09*, 2009.

[67] P. J. Schmid. Dynamic mode decomposition of numerical and experimental data. *submitted to Journal of Fluid Mechanics*, 2009.

[68] P. J. Schmid, K.E. Meyer, and O. Pust. Dynamic mode decomposition and proper orthogonal decomposition of flow in a lid-driven cylindrical cavity. *8th international symposium on particle image velocimetry - PIV09*, 2009.

[69] P. J. Schmid and O. Pust. PIV- and image-based flow analysis of steady and pulsed jet using dynamic mode decomposition. *8th international symposium on particle image velocimetry - PIV09*, 2009.

[70] B. Shapiro. A symmetry approach to extension of flutter boundaries via mistuning. *Journal of Propulsion and Power*, 14(3):354–366, 1998.

[71] S. Shishkin, G. Hagen, and A. Banaszuk. Absolute stability of a reduced order thermo-acoustic model with non-homogeneous wave speed. *Proceedings of the 46th IEEE Conference on Decision and Control*, 2007.

[72] H. Stark and J. W. Woods. *Probability, Random Processes, and Estimation Theory for Engineers.* Prentice Hall, 2nd edition edition, 1994.

[73] K. A. Teerlinck, G. Hagen, A. Banaszuk, J. A. Lovett, J. M. Cohen, A. Ateshkadi, and B. V. Kiel. Demonstration of thermoacoustic instability control in a three-flameholder combustor. *53rd JANNAF (Joint Army-Navy-NASA-Air Force) Propulsion Meeting, Monterey,CA. Dec 5-8*, 2005.

[74] U. Vaidya and G. Hagen. Model reduction of nonlinear systems: Tangent space approach. *Submitted to American Control Conference*, 2010.

[75] J. A. Walker. *Dynamical Systems and Evolution Equations.* Plenum Press, New York, 1980.

[76] Q. Ye, H. Zha, and R.-C. Li. Analysis of an alignment algorithm for nonlinear dimensionality reduction. *BIT Numerical Mathematics*, 47(4):873–885, 2007.

[77] L. Yuan, F. Wen, C. Liu, and H.-Y. Shum. Synthesizing dynamic texture with closed-loop linear dynamic system. pages 603–616. Springer-Verlag, 2004.

[78] H. Zha and Z. Zhang. Spectral properties of the alignment matrices in manifold learning. *SIAM Review*, 51(3):545–566, 2009.

[79] Z. Zhang and H. Zha. Principal manifolds and nonlinear dimension reduction via local tangent space alignment. *SIAM Journal on Scientific Computing*, 26(1):313–338, 2005.

REPORT DOCUMENTATION PAGE

Form Approved
OMB No. 0704-0188

PLEASE DO NOT RETURN YOUR FORM TO THE ABOVE ORGANIZATION.

1. REPORT DATE *(DD-MM-YYYY)*	2. REPORT TYPE	3. DATES COVERED *(From - To)*
07-30-2010	FINAL	April 2007 - July 2010

4. TITLE AND SUBTITLE
DESIGN OF BENEFICIAL WAVE DYNAMICS FOR ENGINE LIFE AND OPERABILITY ENHANCEMENT

5a. CONTRACT NUMBER
FA9550-07-C-0045

5b. GRANT NUMBER
FA9550-07-C-0045

5c. PROGRAM ELEMENT NUMBER

6. AUTHOR(S)
GREGORY HAGEN

5d. PROJECT NUMBER

5e. TASK NUMBER

5f. WORK UNIT NUMBER

7. PERFORMING ORGANIZATION NAME(S) AND ADDRESS(ES)
UNITED TECHNOLOGIES RESEARCH CENTER
411 SILVER LANE
EAST HARTFORD, CT. 06108

8. PERFORMING ORGANIZATION REPORT NUMBER

9. SPONSORING/MONITORING AGENCY NAME(S) AND ADDRESS(ES)
Fariba Fahroo, Ph.D.
Program Manager, Computational Mathematics AFOSR/RSL
875 North Randolph Street
Suite 325, Room 3112

10. SPONSOR/MONITOR'S ACRONYM(S)
AFOSR

11. SPONSOR/MONITOR'S REPORT NUMBER(S)
AFRL-OSR-VA-TR-2012-0080

12. DISTRIBUTION/AVAILABILITY STATEMENT
APPROVED FOR PUBLIC RELEASE

13. SUPPLEMENTARY NOTES

14. ABSTRACT
The objective of this research was to develop techniques for the design of beneficial wave dynamics in jet engines. Our approach focused on symmetry-breaking concepts and stability analysis of systems with mistuning in the presence of feedback nonlinearities. The second part of this research focused on the identification of nonlinear dynamical system models from very high-dimensional data.

15. SUBJECT TERMS
Nonlinear Dynamics, Jet Engines, Thermoacoustic instability, Mistuning, Identification

16. SECURITY CLASSIFICATION OF:			17. LIMITATION OF ABSTRACT	18. NUMBER OF PAGES	19a. NAME OF RESPONSIBLE PERSON
a. REPORT	b. ABSTRACT	c. THIS PAGE			GREGORY HAGEN
SAR	SAR	SAR	SAR		19b. TELEPHONE NUMBER *(Include area code)* 860-610-7794

INSTRUCTIONS FOR COMPLETING SF 298

1. REPORT DATE. Full publication date, including day, month, if available. Must cite at least the year and be Year 2000 compliant, e.g. 30-06-1998; xx-06-1998; xx-xx-1998.

2. REPORT TYPE. State the type of report, such as final, technical, interim, memorandum, master's thesis, progress, quarterly, research, special, group study, etc.

3. DATES COVERED. Indicate the time during which the work was performed and the report was written, e.g., Jun 1997 - Jun 1998; 1-10 Jun 1996; May - Nov 1998; Nov 1998.

4. TITLE. Enter title and subtitle with volume number and part number, if applicable. On classified documents, enter the title classification in parentheses.

5a. CONTRACT NUMBER. Enter all contract numbers as they appear in the report, e.g. F33615-86-C-5169.

5b. GRANT NUMBER. Enter all grant numbers as they appear in the report, e.g. AFOSR-82-1234.

5c. PROGRAM ELEMENT NUMBER. Enter all program element numbers as they appear in the report, e.g. 61101A.

5d. PROJECT NUMBER. Enter all project numbers as they appear in the report, e.g. 1F665702D1257; ILIR.

5e. TASK NUMBER. Enter all task numbers as they appear in the report, e.g. 05; RF0330201; T4112.

5f. WORK UNIT NUMBER. Enter all work unit numbers as they appear in the report, e.g. 001; AFAPL30480105.

6. AUTHOR(S). Enter name(s) of person(s) responsible for writing the report, performing the research, or credited with the content of the report. The form of entry is the last name, first name, middle initial, and additional qualifiers separated by commas, e.g. Smith, Richard, J, Jr.

7. PERFORMING ORGANIZATION NAME(S) AND ADDRESS(ES). Self-explanatory.

8. PERFORMING ORGANIZATION REPORT NUMBER. Enter all unique alphanumeric report numbers assigned by the performing organization, e.g. BRL-1234; AFWL-TR-85-4017-Vol-21-PT-2.

9. SPONSORING/MONITORING AGENCY NAME(S) AND ADDRESS(ES). Enter the name and address of the organization(s) financially responsible for and monitoring the work.

10. SPONSOR/MONITOR'S ACRONYM(S). Enter, if available, e.g. BRL, ARDEC, NADC.

11. SPONSOR/MONITOR'S REPORT NUMBER(S). Enter report number as assigned by the sponsoring/ monitoring agency, if available, e.g. BRL-TR-829; -215.

12. DISTRIBUTION/AVAILABILITY STATEMENT. Use agency-mandated availability statements to indicate the public availability or distribution limitations of the report. If additional limitations/ restrictions or special markings are indicated, follow agency authorization procedures, e.g. RD/FRD, PROPIN, ITAR, etc. Include copyright information.

13. SUPPLEMENTARY NOTES. Enter information not included elsewhere such as: prepared in cooperation with; translation of; report supersedes; old edition number, etc.

14. ABSTRACT. A brief (approximately 200 words) factual summary of the most significant information.

15. SUBJECT TERMS. Key words or phrases identifying major concepts in the report.

16. SECURITY CLASSIFICATION. Enter security classification in accordance with security classification regulations, e.g. U, C, S, etc. If this form contains classified information, stamp classification level on the top and bottom of this page.

17. LIMITATION OF ABSTRACT. This block must be completed to assign a distribution limitation to the abstract. Enter UU (Unclassified Unlimited) or SAR (Same as Report). An entry in this block is necessary if the abstract is to be limited.